



**HAL**  
open science

## Gypsum on Mars: A Detailed View at Gale Crater

David Vaniman, Steve Chipera, Elizabeth Rampe, Thomas Bristow, David Blake, Johannes Meusbürger, Tanya Peretyazhko, William Rapin, Jeff Berger, Douglas Ming, et al.

► **To cite this version:**

David Vaniman, Steve Chipera, Elizabeth Rampe, Thomas Bristow, David Blake, et al.. Gypsum on Mars: A Detailed View at Gale Crater. *Minerals*, 2024, 14 (8), pp.815. 10.3390/min14080815 . hal-04767660

**HAL Id: hal-04767660**

**<https://hal.science/hal-04767660v1>**













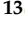

Submitted on 5 Nov 2024

**HAL** is a multi-disciplinary open access archive for the deposit and dissemination of scientific research documents, whether they are published or not. The documents may come from teaching and research institutions in France or abroad, or from public or private research centers.

L'archive ouverte pluridisciplinaire **HAL**, est destinée au dépôt et à la diffusion de documents scientifiques de niveau recherche, publiés ou non, émanant des établissements d'enseignement et de recherche français ou étrangers, des laboratoires publics ou privés.

## Article

# Gypsum on Mars: A Detailed View at Gale Crater

David Vaniman <sup>1,\*</sup>, Steve Chipera <sup>1</sup>, Elizabeth Rampe <sup>2</sup>, Thomas Bristow <sup>3</sup>, David Blake <sup>3</sup>, Johannes Meusbürger <sup>3</sup>, Tanya Peretyazhko <sup>4</sup>, William Rapin <sup>5</sup>, Jeff Berger <sup>4</sup>, Douglas Ming <sup>2</sup>, Patricia Craig <sup>1</sup>, Nicholas Castle <sup>1</sup>, Robert T. Downs <sup>6</sup>, Shaunna Morrison <sup>7</sup>, Robert Hazen <sup>7</sup>, Richard Morris <sup>2</sup>, Aditi Pandey <sup>2,8</sup>, Allan H. Treiman <sup>8</sup>, Albert Yen <sup>9</sup>, Cherie Achilles <sup>10</sup>, Benjamin Tutolo <sup>11</sup>, Elisabeth Hausrath <sup>12</sup>, Sarah Simpson <sup>2</sup>, Michael Thorpe <sup>13</sup>, Valerie Tu <sup>4</sup>, David J. Des Marais <sup>3</sup>, John Grotzinger <sup>14</sup> and Abigail Fraeman <sup>9</sup>

- <sup>1</sup> Planetary Science Institute, Tucson, AZ 85719, USA; steve.chipera@gmail.com (S.C.); pcraig@psi.edu (P.C.); ncastle@psi.edu (N.C.)
  - <sup>2</sup> NASA Johnson Space Center, Houston, TX 77058, USA; elizabeth.b.rampe@nasa.gov (E.R.); douglas.w.ming@nasa.gov (D.M.); richard.v.morris@nasa.gov (R.M.); aditi.pandey@nasa.gov (A.P.); sarah.l.simpson@nasa.gov (S.S.)
  - <sup>3</sup> NASA Ames Research Center, Moffett Field, CA 94043, USA; thomas.f.bristow@nasa.gov (T.B.); david.blake@nasa.gov (D.B.); johannes.m.meusbuerger@nasa.gov (J.M.); david.j.desmarais@nasa.gov (D.J.D.M.)
  - <sup>4</sup> Jacobs JETSII, NASA Johnson Space Center, Houston, TX 77058, USA; tanya.peretyazhko@nasa.gov (T.P.); jeff.berger@nasa.gov (J.B.); valerie.m.tu@nasa.gov (V.T.)
  - <sup>5</sup> Institut de Recherche en Astrophysique et Planétologie, 31400 Toulouse, France; william.rapin@irap.omp.eu
  - <sup>6</sup> Department of Geosciences, University of Arizona, Tucson, AZ 85721, USA; rdowns@arizona.edu
  - <sup>7</sup> Carnegie Institute for Science, Washington, DC 20015, USA; smorrison@carnegiescience.edu (S.M.); rhazen@carnegiescience.edu (R.H.)
  - <sup>8</sup> The Lunar and Planetary Institute, Houston, TX 77058, USA; treiman@lpi.usra.edu
  - <sup>9</sup> Jet Propulsion Laboratory, California Institute of Technology, Pasadena, CA 91011, USA; albert.s.yen@jpl.nasa.gov (A.Y.); abigail.a.fraeman@jpl.nasa.gov (A.F.)
  - <sup>10</sup> NASA Goddard Space Flight Center, Greenbelt, MD 20771, USA; cherie.n.achilles@nasa.gov
  - <sup>11</sup> Department of Earth, Energy, and Environment, University of Calgary, Calgary, AB T2N 1N4, Canada; benjamin.tutolo@ucalgary.ca
  - <sup>12</sup> Department of Geoscience, University of Nevada, Las Vegas, NV 89154, USA; elisabeth.hausrath@unlv.edu
  - <sup>13</sup> Goddard Space Flight Center, CRESST II, University of Maryland, Greenbelt, MD 20771, USA; michael.t.thorpe@nasa.gov
  - <sup>14</sup> Division of Geologic and Planetary Sciences, California Institute of Technology, Pasadena, CA 91125, USA; grotz@gps.caltech.edu
- \* Correspondence: dvaniman@psi.edu



**Citation:** Vaniman, D.; Chipera, S.; Rampe, E.; Bristow, T.; Blake, D.; Meusbürger, J.; Peretyazhko, T.; Rapin, W.; Berger, J.; Ming, D.; et al. Gypsum on Mars: A Detailed View at Gale Crater. *Minerals* **2024**, *14*, 815. <https://doi.org/10.3390/min14080815>

Academic Editors: Alessandra Costanzo and Mara Cipriani

Received: 17 July 2024

Revised: 4 August 2024

Accepted: 6 August 2024

Published: 12 August 2024



**Copyright:** © 2024 by the authors. Licensee MDPI, Basel, Switzerland. This article is an open access article distributed under the terms and conditions of the Creative Commons Attribution (CC BY) license (<https://creativecommons.org/licenses/by/4.0/>).

**Abstract:** Gypsum is a common mineral at Gale crater on Mars, currently being explored by the Mars Science Laboratory (MSL) rover, *Curiosity*. In this paper, we summarize the associations of gypsum with other sulfate minerals (bassanite, anhydrite, jarosite, starkeyite, and kieserite) from the lowest levels of the crater’s northern moat zone (Aeolis Palus) up through ~0.8 km of the stratigraphic section in the lower slopes of the sedimentary mound developed around the central peak, Aeolis Mons (informally, Mount Sharp). The analysis is based on results from the CheMin X-ray diffraction instrument on *Curiosity*, supplemented with information from the rover’s versatile instrument suite. Gypsum does not occur with the same frequency as less hydrous Ca-sulfates, likely, in most cases, because of its dehydration to bassanite and possibly to anhydrite. All three of these Ca-sulfate phases often occur together and, along with other sulfates, in mixed assemblages that are evidence of limited equilibration on a cold, dry planet. In almost all samples, at least one of the Ca-sulfate minerals is present, except for a very limited interval where jarosite is the major sulfate mineral, with the implication of more acidic groundwater at a much later time in Gale crater’s history. Although observations from orbit reveal a sulfate-rich surface, currently active dark basaltic dunes at Gale crater have only small amounts of a single sulfate mineral, anhydrite. Gale crater has provided the most complete mineralogical analysis of a site on Mars so far, but the data in hand show that Gale crater mineralogy is not a blueprint with planet-wide application. The concurrent study of Jezero crater by the Mars 2020 mission and comparisons to what is believed to be the most extensive

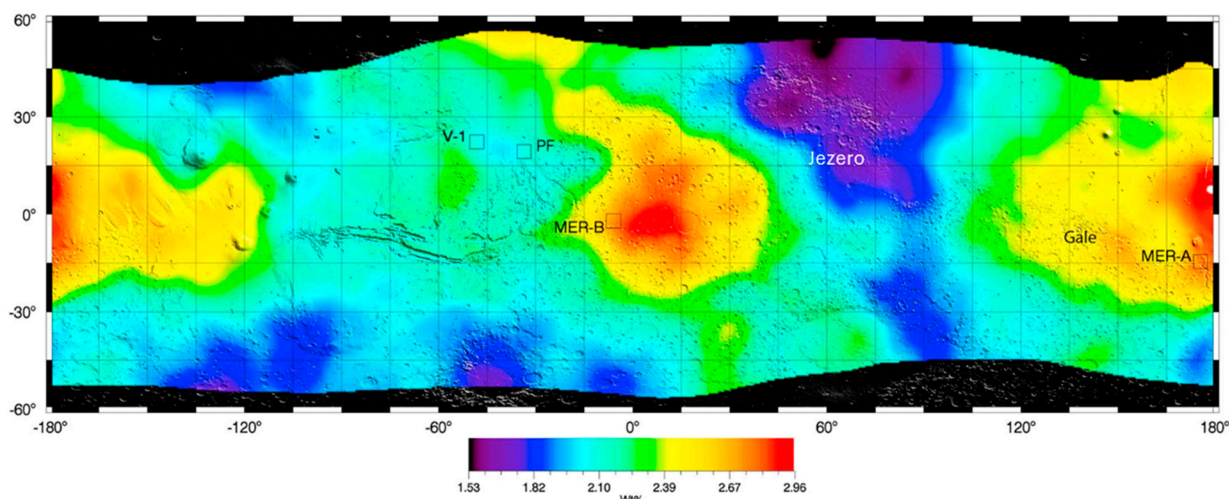
deposit of gypsum on Mars, in the dune fields at the north polar ice cap, show significant diversity. Unraveling the stories of gypsum and other sulfates on Mars is just beginning.

**Keywords:** Mars; gypsum; sulfate

## 1. Introduction

Gypsum is a common mineral on Mars, occurring in diverse settings. It is widespread, from gypsum dunes near the North Polar Cap to near-equatorial fracture fillings and sediments. The detection and mapping of surface gypsum on Mars have been pursued planet-wide by orbital spectrometers, notably the ESA's Mars Express Observatoire pour la Mineralogie, l'Eau, les Glaces et l'Activité (OMEGA) instrument [1] and NASA's Mars Reconnaissance Orbiter Compact Reconnaissance Imaging Spectrometer for Mars (CRISM) instrument [2]. The OMEGA instrument has been in orbit around Mars since 2003, and CRISM since 2006. Orbital instruments are sensitive to reflected light in the visible and near-infrared (VNIR) range: OMEGA at 0.35–5.1  $\mu\text{m}$  and CRISM at 0.362–3.92  $\mu\text{m}$ . These spectral ranges detect the structural setting of water molecules (and hydroxyl) in hydrous minerals, making them effective at identifying salt hydrates. Gypsum, with two waters of hydration, falls within a group referred to as "polyhydrated sulfates" that includes multiple hydration states of Fe-sulfates and Mg-sulfates that are also found on Mars. In many cases, the explicit mineral cannot be specified, and the "polyhydrated sulfate" term is used instead. VNIR spectra are also effective at identifying monohydrates (such as kieserite [3]) and subhydrates (such as bassanite [4]). They are not effective at detecting anhydrous salts such as anhydrite. The sulfate salt surficial reflectance seen from orbit, if not a generic "polyhydrated sulfate", is most often classified within the area of any given spectral instrument's spatial resolution (e.g., ~18 m diameter for CRISM targeted data) as a specific salt hydrate mineral that dominates the reflectance (gypsum, bassanite, kieserite, szomolnokite, etc.). Mineral maps and associations on the ground, where resolution is significantly greater, are more complex. In this paper, we show that gypsum at our Mars field site, Gale crater, is never the sole Ca-sulfate and is typically accompanied by bassanite and/or anhydrite (as well as other sulfate salts).

Gale crater is the site that was selected for the Mars Science Laboratory (MSL) rover *Curiosity*. This crater, ~150 km in diameter, is located near the equator of Mars (5.4° S, 137.8° E) along a physiographic feature noted as the "dichotomy boundary" between the ancient, heavily cratered southern highlands and the younger surfaces of the northern lowlands. Figure 1, adapted from [5], shows the location of Gale crater on a map of sulfur concentrations in the upper few decimeters of the Martian surface, based on the 2001 Mars Odyssey gamma ray spectrometer (GRS) experiment (the data do not extend above ~50° latitude because permafrost interferes with the method). Energetic cosmic rays penetrate several tens of centimeters into the surface; as a result, the sulfur data represent the subsurface to decimeter-scale depths, unlike surficial spectral reflectance. The map in Figure 1 shows several enrichments of sulfur concentrations at near-equatorial latitudes, with a notable maximum in the broad region that includes Gale crater. Gale crater is thus situated at one of the best locations for examining sulfate minerals on Mars. Gale was chosen as the MSL landing site because sediments of the large (5.5 km high) central peak within the crater record a major transition in the environment of Mars, from a past marked by clays and other silicate and oxide minerals indicative of a wetter environment to a drier sulfate-rich environment [6,7]. Gypsum is an important part of the later sulfate history but also has a significant role in sediments stratigraphically below the sulfate-rich zone.



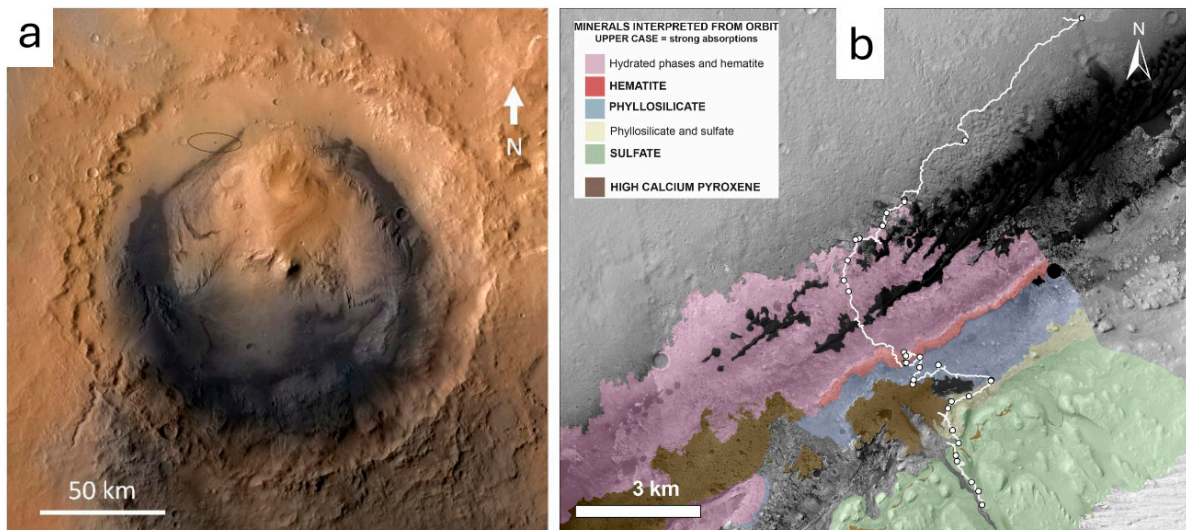
**Figure 1.** Sulfur abundance in the upper ~1 to 2 dm of the Martian surface, based on the 2001 Mars Odyssey mission orbital gamma ray spectrometer (GRS), adapted from [5]. Labeled on the map are Gale and Jezero craters, as well as the landing sites of earlier missions: MER-A (the Spirit rover), MER-B (the Opportunity rover), PF (Pathfinder), and V-1 (Viking lander 1). No data are available at higher latitudes, where permafrost ice precludes sulfur data detection by the GRS.

Figure 2 shows a closer view of Gale crater from orbit, with a detailed view of the rover traverse from the landing ellipse onto the lower slopes of Mount Sharp. The total distance of the traverse at the time this figure was generated was ~11 km, with an elevation rise of ~0.8 km; the path of the rover from the landing site in Aeolis Palus to Mount Sharp is shown in white, with black circles showing where the rover paused to collect samples. The colors in this figure, based on CRISM spectral analysis, delineate a sequence of zones of CRISM-determined mineralogy ascending the lower sediments of Mount Sharp. Passing from the floor of the crater where the CRISM spectra were nondescript (gray), the rover entered sediments of the lower Murray formation (plum color), an erosionally resistant rise (Hematite Ridge, in red tones), sediments of the Carolyn Shoemaker formation (blue), a transition zone of diminishing clay mineral abundance and increasing sulfate minerals (Carolyn Shoemaker to Mirador formations, blue to pale green), and the Mg-sulfate-bearing unit (green). Attempts to drive onto a rugged terrain of debris rich in high-Ca pyroxene (brown) were unsuccessful, so sampling of that unit was limited.

The sulfate mineralogy at Gale crater discussed in this paper was determined by X-ray diffraction (XRD) using the CheMin diffractometer carried by the *Curiosity* rover. CheMin samples include scooped sands or, more typically, drill powders of sedimentary rock, collected at a depth of a few centimeters. A major goal of the MSL mission at Gale crater is to traverse and examine the lower slopes of Mount Sharp, from sediments with abundant clay minerals up into the higher Mg-sulfate-bearing unit that appears to represent a significant shift to a drier climate [6,8]. The Mg-sulfate-bearing unit is distinguished by the appearance of magnesium sulfate minerals (starkeyite and kieserite [9]), but calcium sulfate minerals are common below and above this transition.

As noted above, gypsum at Gale crater is found in close association with both bassanite and anhydrite [10]. All three minerals are readily detected, and their abundances quantified, with XRD; gypsum and bassanite are especially detectable, as they have prominent diffraction maxima at low 2-theta where there are few interfering peaks from other minerals. All three of the Ca-sulfates have CheMin detection limits below 1 wt%, which are, for most samples, their abundance quantitation limits. The CheMin data for anhydrite are crucial because, as noted above, it is a water- and hydroxyl-free mineral that is invisible to remote spectral analysis; thus, the CheMin dataset is unique for Mars by including all three major Ca-sulfate phases.





**Figure 2.** (a) Color image of Gale crater from orbit. The “engineering confidence” landing zone of the MSL rover is shown as a black ellipse in Aeolus Palus, the lowland north of Mount Sharp. The elevation of Mount Sharp above the landing zone is ~5.5 km. (b) The traverse (white path) of the MSL rover *Curiosity* out of the landing zone and onto the lower slopes of Mount Sharp. Sampling locations along the traverse are shown with black circles (see the text for further explanation of the colored units). The elevation rise from the first sampling point in Aeolus Palus to the last sampling point shown is ~790 m.

## 2. Methods

### 2.1. X-Ray Diffraction, with Evidence of Gypsum Dehydration to Bassanite

The CheMin instrument uses a Co anode X-ray tube with a nominal operating voltage of 28 keV, a filament current of 1.5 A, and a cathode output of 100  $\mu$ A (see [11] for a detailed instrument description and a summary of current results at Gale crater). Powder samples (<150  $\mu$ m grain size) of ~50 mm<sup>3</sup> volume are delivered to CheMin analysis cells that have either Mylar or Kapton windows. Reusable sample cells are mounted on a vertical rotating sample wheel; the analyzed samples are dumped by inverting the wheel and piezoelectrically shaking the used cell. Loaded cells are also shaken during analysis to randomize grain orientations. Energy resolution is used to differentiate fluoresced and diffracted photons striking the CCD detector; fluoresced photons provide some XRF data, and the two-dimensional (2D) positions of diffracted Co K $\alpha$  photons are used to construct a diffraction pattern. The circumferential integration of Debye diffraction rings, adjusted for arc length, produces a conventional 1D XRD pattern with a  $2\theta$  resolution of ~0.3° and a  $2\theta$  range of 2 to 52 degrees. The positions of diffracted photons are summed over repeated 10 s measurements for several hours during each night of analysis. The base of the sample cell is locked in place during analysis, and the sample-to-detector distance is determined to a higher precision using the best fit to plagioclase  $c$  and  $\gamma$  cell parameters [12,13]. The abundances of crystalline phases are determined by full-pattern fitting and Rietveld analysis; the abundances of amorphous components and poorly crystalline minerals (clay minerals and opal-CT) are determined using the program FULLPAT [14]. All abundances cited in this paper are in weight percent of the combined crystalline and amorphous materials in each sample.

On Mars, adaptations had to be made as experience was gained and systems aged. For the first years of operation at Gale crater, all samples delivered to CheMin were sieved to <150  $\mu$ m, moving powder by hammering vibrations of the locked drill as a series of sieves was rotated into position [15]. For many sols (Martian days), this system worked as intended. After drilling at the site called Sebina, around sol 1496 of the mission, it was found that the brake assembly that locked the drill for hammering while drilling or sieving was in danger of failing to release, which would prevent all future drill sampling. An

ingenious engineering solution was developed: feed-extended drilling, which moves the drill assembly out beyond its stabilizing prongs, followed by feed-extended sample transfer, which delivers the sample directly to CheMin by bypassing the sieve assembly and simply back-rotating the drill auger over the CheMin inlet. Although this no longer allows use of the sieve system, all drill samples since Sebina have provided material fine enough to facilitate good diffraction. Also, in the first years of operation, samples were analyzed over several nights, spaced at time intervals determined by the rover's energy budget, allowance for operating other instruments, and other operational considerations. Later, as some cells were becoming harder to dump for subsequent samples, shorter analyses to prevent sample packing, sometimes a single night, have been used with very little degradation of mineral detection. Finally, the analysis of the first gypsum-bearing sample, Oudam (on sol 1361), revealed that after the first night of analysis, the warm daytime temperature inside CheMin (up to about 30 °C) caused gypsum to dehydrate to bassanite over several sols. The solution adopted was to base gypsum and bassanite abundances on the first night of analysis, before the sample in the cell experienced a day cycle [10]. This method has worked well for all gypsum-bearing samples analyzed by CheMin, as well as for the Mg-sulfate mineral starkeyite, which is similarly prone to dehydration [9].

Dehydration of gypsum to bassanite inside CheMin provides important information about how close gypsum is to instability at the Mars equatorial surface. The temperature difference from sampling to analysis in the CheMin instrument is notable, ranging from  $< \sim 253$  K at sample depth to temperatures inside CheMin that range from  $\sim 280$  K at night to  $\sim 300$  K at midday. The dehydration process is detailed for earlier samples in [10], but an exceptionally good analysis of the full process was obtained with the more recent sample Zechstein (Figure 3), where the drill penetrated a gypsum vein with exceptionally high gypsum abundance (18%, versus the previous highest abundance of 3%). Figure 3 shows the loss of gypsum with formation of bassanite over a period of  $\sim 38$  sols, illustrated by gradual loss of intensity in the gypsum 020 and 021 diffraction peaks as the combined bassanite 200/110 peak increased. In previous samples with less gypsum, complete conversion to bassanite occurred within  $\sim 5$ – $10$  sols; the fixed parameter of the narrow inlet to CheMin analysis cells ( $6 \text{ mm} \times 175 \text{ }\mu\text{m}$ ) limits the rate of dehydration, as does the variable parameter of gypsum abundance. Dehydration of gypsum to bassanite also occurs on exposed surfaces at Gale crater; evidence of this effect is provided by laser ablation measurements of hydrogen content at the surface with the ChemCam instrument on MSL, which found abundant bassanite but no gypsum [16]. With slow erosion rates on Mars, eons of surface exposure to midday temperatures, and with surface winds to aid desiccation, near-equatorial locations such as Gale crater favor dehydration of gypsum to form bassanite [17].

An important aspect of the diffraction shown in Figure 3 is a fortuitous absence: over the broad range of  $\text{Co K}\alpha$  2-theta angles shown, there are no significant peaks from any minerals besides gypsum and bassanite. In some samples from Gale crater, feldspars and pyroxenes have significant peaks at  $\sim 16^\circ$  2-theta, but these are clearly separated from the bassanite peak at  $17^\circ$ . With no interference from other minerals, this “Ca-sulfate window” makes the detection limits for gypsum and bassanite very low, with quantitation effective down to  $\sim 0.4$  wt%. In this paper, we focus on the distribution and abundance of Ca-sulfates, particularly gypsum, but the CheMin diffraction data provide quantitative abundances for the full suite of crystalline silicate, oxide, oxyhydroxide, sulfate, carbonate, and phosphate minerals, as well as abundance information on non-crystalline materials. All diffraction data are available in the Planetary Data System (<https://pds.nasa.gov>, (accessed on 26 June 2024), and in two databases that are more focused on MSL, the CheMin Database (<https://odr.io/CheMin#/search/display/84/eyJkdF9pZCI6IjZlIn0/1>, (accessed on 20 June 2024) and the Gale Crater Mineralogy and Geochemistry Database (<https://doi.org/10.48484/JN48-YW52>, (accessed on 20 June 2024).

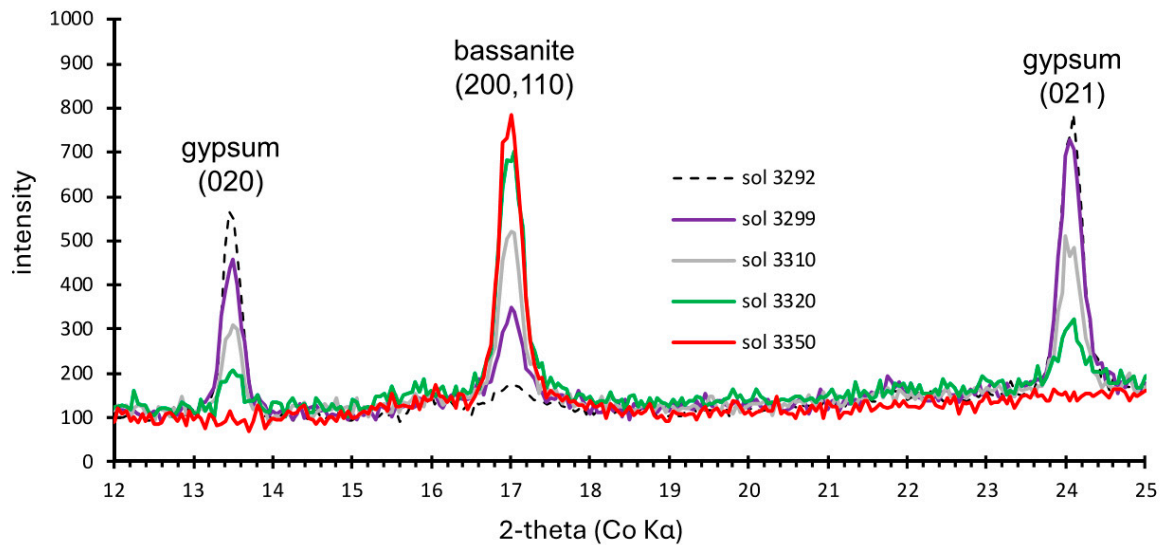


**Figure 3.** CheMin X-ray diffraction data from the Zechstein sample on five separate nights, from MSL mission sols (operational Mars days) 3292 to 3350. The drill at Zechstein penetrated a buried vein of pure or almost pure gypsum; a small amount of initial bassanite may be in the rock matrix above the vein rather than within the vein. Diffraction data illustrate the progressive transformation of gypsum into bassanite inside the CheMin sample cell.

## 2.2. APXS

*Curiosity's* Alpha Particle X-ray Spectrometer (APXS) provides chemical data that are complementary to CheMin. In particular, the APXS quantifies sulfur and common sulfate cations (e.g., Ca, Mg). The APXS uses X-ray fluorescence and Particle-Induced X-ray Emission (PIXE) spectrometry to analyze major, minor, and selected trace elements with atomic weights  $\geq 11$  (i.e., sodium) in rocks and soils [18,19]. The  $\sim 2$  cm field of view typically represents the bulk composition of a target, and when deployed over drilled fines, the APXS provides, in most cases, a reasonably accurate bulk analysis of the samples delivered to CheMin. This enables correlation of the mineralogy determined by CheMin to the chemical composition determined by the APXS. Thus, the sulfate mineralogy analyzed in dozens of CheMin samples can be interpreted in relation to the sulfur content of hundreds of targets measured by the APXS.

## 2.3. ChemCam

ChemCam is a laser-induced breakdown spectrometer (LIBS) instrument that provides elemental abundance analyses with a spot size of 300 to 500  $\mu\text{m}$  in diameter, as well as detailed images using its remote micro-imager (RMI) [20]. The LIBS technique measures major elements and a number of minor and trace elements. In particular, it is uniquely sensitive to hydrogen. A series of laser shots are typically obtained at each of 5 to 10 points on a target, ablating and excavating within a hundred-micron-scale depth from the surface, depending on material strength. Major element contents for each point were obtained using the current calibration model [21]. Water and sulfate contents can be estimated using dedicated calibration models: for water content, quantification uses the hydrogen signal [22], and for sulfate content, the sulfur signal is used with in situ calibration, as described in [23] for sulfate enrichments in the Murray formation. This unique combination of sulfur and hydrogen contents from in situ measurements can be used to assess the hydration state of sulfate minerals exposed at Mars' surface without drilling and sample handling. The dataset now includes more than 30 k points on targets along the rover traverse.

### 3. Discussion: Mineralogy in Stratigraphic Context at Gale Crater

#### 3.1. Stratigraphic Overview

Figure 4 places the samples discussed in this paper in relative elevation against the MSL mission timeline, from the first sampling campaign, a scoop sample of the Rocknest eolian deposit on sol 94 (94 Mars days after landing), through analysis of the drill sample at Mineral King on sol 4110. Progress has been generally upward, with some reversals due to small terrain effects, as at Vera Rubin Ridge and a short climb to sample at the Edinburgh drill site. Strata at Gale crater are mostly flat-lying or have gentle dips (~2° to 4° [7]), so elevation is a reasonable proxy for the stratigraphic sequence.

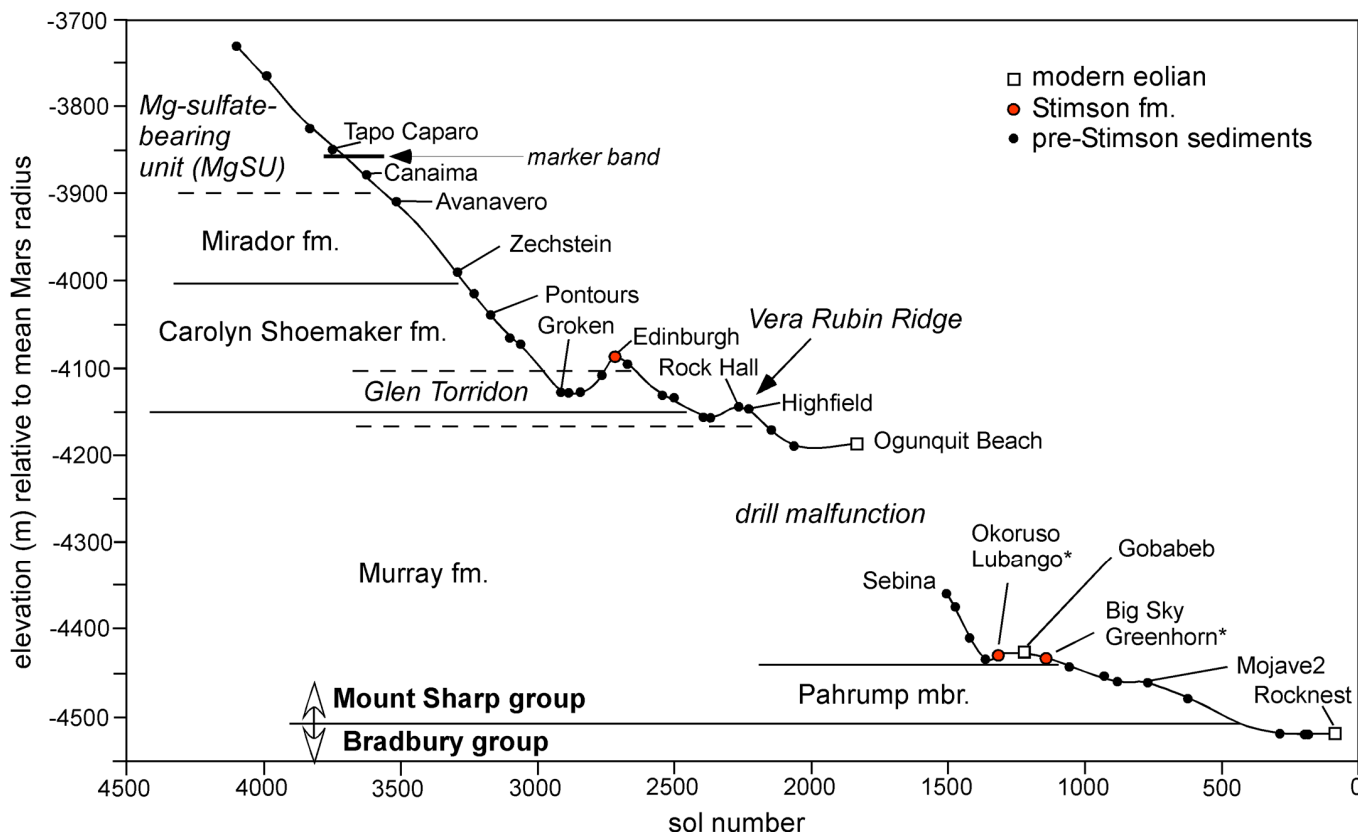


**Figure 4.** Positions of CheMin X-ray diffraction samples, plotted against depth (m) below the mean Mars radius and MSL mission day (sol) at the analysis location. Drill samples from the Bradbury and Mount Sharp groups are marked as black circles, those from the unconformably overlying Stimson formation as red circles, and scoop samples of modern eolian sands as open squares. Stratigraphic units are separated by solid lines; dashed lines mark the extent of the Glen Torridon unit and the lower boundary of the Mg-sulfate-bearing unit. Asterisks (\*) mark samples where fracture-filling minerals are abundant. Informal units and annotations are in italics. Selected samples are labeled for comparison with Figure 5.

Figure 5 places gypsum at Gale crater in a stratigraphic context and in association with other sulfate minerals. The stratigraphy extends from the MSL landing site in the topographically and stratigraphically lowest levels of Gale crater (Aeolis Palus) onto the north flank of the crater’s central mound that forms Mount Sharp. The Bradbury group represents sediments sampled during the traverse from the landing site toward Mount Sharp.



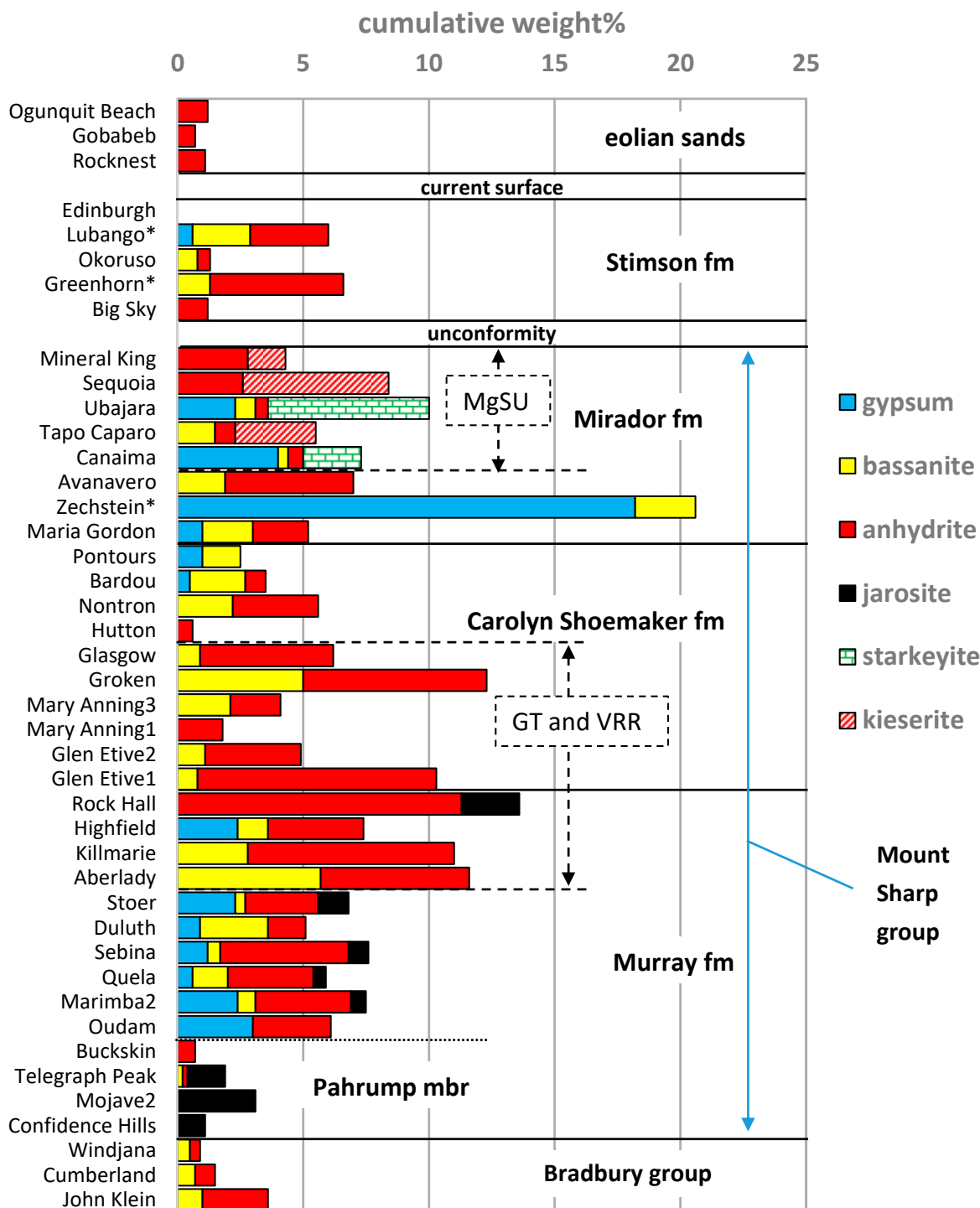


**Figure 5.** The cumulative weight percentage of sulfate minerals in all samples analyzed to date by XRD at Gale crater. Samples in the bottom panel are in relative stratigraphic elevation from the landing site up to Mineral King. The panel labeled Stimson represents younger samples above an unconformity at the top of the Mount Sharp group. Asterisks mark samples of later vein fillings in the Stimson that cross the unconformity, as well as the Zechstein sample that contains a major gypsum vein. The upper panel represents modern eolian sands. Abbreviations are for the Glen Torridon (GT), Vera Rubin Ridge (VRR), and the Mg-sulfate-bearing unit (MgSU) of the upper Mount Sharp group. For details of data collection, XRD pattern processing, and a compilation of full mineralogical and crystal-chemical analyses, refer to [11–13].

Although the discoveries made at Yellowknife Bay were profoundly important to mission success [24,25], the sampling frequency in the broader Bradbury group was minimal due to the need to drive expeditiously to higher stratigraphic levels of the Mount Sharp group, where important mineral signatures were observed from orbit. From the lowermost slopes of Mount Sharp up to the current rover position, the mission has been ascending through sediments of the Mount Sharp group, represented in Figure 5 by strata extending from Pahrump through the Mg-sulfate-bearing unit. Although diagenetic mineralogy varies considerably in the Mount Sharp group, the overall plagioclase (andesine) and pyroxene (augite, pigeonite, and orthopyroxene) detrital mineral composition has remained fairly consistent [12,13], dominated by phases derived from basaltic to intermediate volcanic sources. Olivine (forsterite, Fo ~60) is common throughout the Bradbury group and in much of the lower Mount Sharp group from the Pahrump member up to Sebina, but above Sebina olivine is not detected in the Mount Sharp group. We interpret the loss of olivine as evidence of extensive weathering throughout the Mount Sharp group, either at the point of provenance or during transport, deposition, and diagenesis, assuming olivine to be common to most basaltic sources at Gale crater. This alteration of the Mount Sharp group contrasts with evidence for olivine retention in younger rocks and sediments; for example, there is abundant olivine in at least part of the unconformably overlying, much younger Stimson formation (in the Edinburgh sample) and in all modern eolian sands of the crater. The abundance of olivine in younger sediments suggests that more extensive alteration of olivine in the Mount Sharp group occurred in earlier sedimentation and especially in diagenetic processes.

Sampling of the Stimson formation has been limited to two localities. One locality, at the Naukluft Plateau, had extensive silicic/sulfate alteration zones (~25 cm wide) in fractures that allowed paired drill sampling of both alteration and wall rock (paired samples Lubango\*/Okoruso and Greenhorn\*/Big Sky, where an asterisk signifies the fracture alteration-zone sample). The phases formed along the fracture walls include amorphous silica, as well as anhydrite, bassanite, and lesser gypsum. The other Stimson locality, at Siccar Point (sample Edinburgh), had no sulfate minerals and abundant (8%) olivine, suggesting minimal alteration; the absence of olivine at the Naukluft Plateau may indicate broader alteration beyond the obvious wall-rock zone. The Stimson is a complex unit with variable alteration, but the few samples limit interpretation.

Scoop sampling of loose sands was used for the first analysis on another planet by XRD: Rocknest, an inactive eolian deposit [26]. Later, CheMin analyzed two representative samples from active dune fields: Gobabeb and Ogunquit Beach [27,28]. The sand samples contain minimal amounts of crystalline sulfates, ~1% by mass of anhydrite. No gypsum or bassanite, nor other sulfate minerals, have been detected in these dark sands.

The most complete set of data on gypsum and associated sulfate minerals within contiguous stratigraphy is that of the Bradbury and Mount Sharp groups, from the John Klein to Mineral King sampling sites (Figure 5). The Bradbury group is sparsely represented by just three samples: two similar mudstones of basaltic provenance drilled close together (John Klein and Cumberland, ref. [24,25]) and a distinctive potassic basaltic sandstone (Windjana, ref. [29]) with abundant sanidine, the like of which has not been seen since. Small amounts of bassanite and anhydrite occur in all three of these samples as late diagenetic alteration. In the mudstones of John Klein and Cumberland, although no gypsum was observed by XRD, the Mastcam instrument on MSL provided spectral hydration-index measurements consistent with the presence of gypsum in veins crossing the mudstone [25], suggesting that the vein system of the deepest mudstones at Gale crater might contain all three of the principal Ca-sulfates. ChemCam has been able to document nearly pure Ca-sulfate compositions in numerous fracture-fill veins along its traverse, and the hydrogen signal points to a predominantly bassanite hydration state (Figure 6), likely formed by dehydration of gypsum [16]. These Ca-sulfate veins have also been observed with chemical trends suggesting that Ca-sulfates (likely gypsum at depth) are locally mixed with Fe/Mg-bearing oxides or sulfates [30]. Gypsum is thus likely to extend throughout the Bradbury

and Mount Sharp groups in the form of veins, with the greatest abundance in light-toned fractures that were not sampled by the MSL drill for XRD analysis.

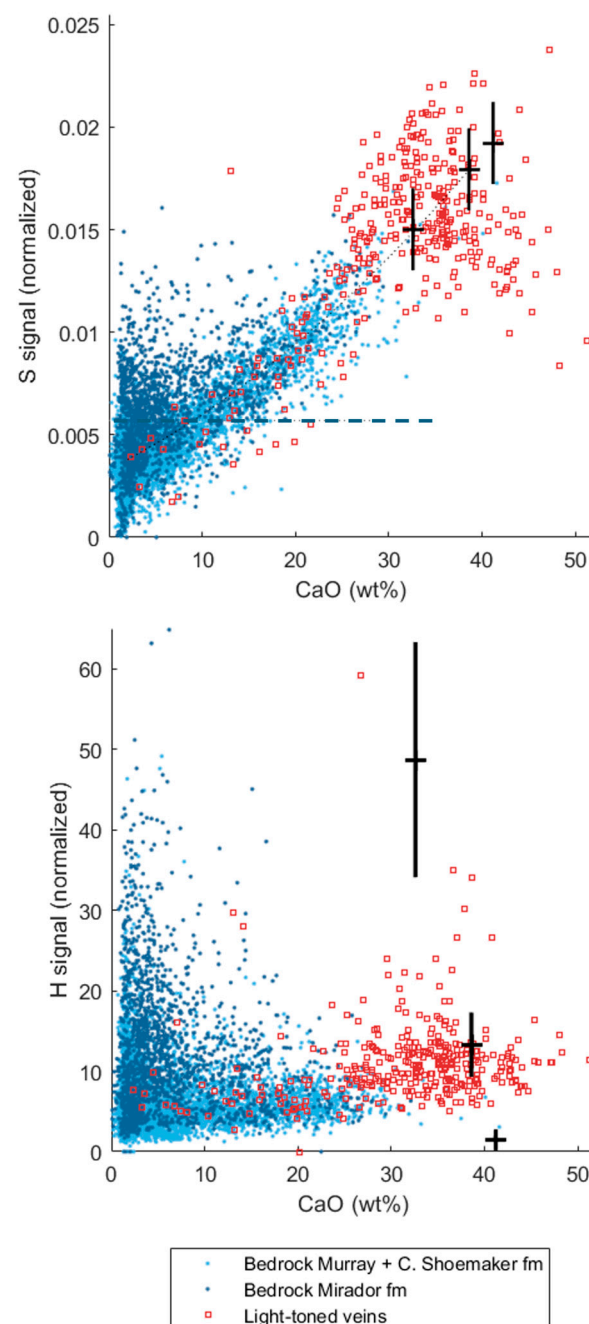


**Figure 6.** A summary of ChemCam analyses showing S and H signals as a function of CaO content on Mount Sharp group bedrock below the Mirador formation (pale blue), above it (dark blue), and for light-toned vein-fill material identified throughout. The sulfur signal limit of detection is shown as a horizontal dashed line,  $\text{SO}_3 > 10 \text{ wt}\%$  (**top**), and end-members (black crosses) represent gypsum, bassanite, and anhydrite. Vertical error bars on end-members represent sulfate (**top**) and water content (**bottom**) calibration uncertainties.

The vast majority of samples analyzed by CheMin over the 12 years of the mission have been of rocks from the Mount Sharp group. The major mineralogical makeup of Mount Sharp group sediments, in weight percent, averages approximately 43% X-ray amorphous material, 24% feldspar (21% andesine, 3% sanidine), 17% clay minerals, 8% Fe-oxides (5% hematite, 3% magnetite), 6% pyroxene, 4% anhydrite, 3% gypsum, 2% bassanite,

and 1% olivine (Fe-forsterite). Less common minerals, locally present in minor amounts up to several percent, include the sulfate mineral jarosite and the non-sulfates goethite, akaganeite, quartz, cristobalite, opal-A, opal-CT, tridymite, apatite, and Fe-carbonates (siderite and/or ankerite). Between the samples Avanavero and Canaima, the MSL mission entered the mineralogically distinct Mg-sulfate-bearing unit where minerals excluded from the average percentages above, the Mg-sulfates starkeyite and kieserite and the Fe-carbonate mineral siderite, are present at several percent. The appearance of Mg-sulfates in sediments is associated with a major transition in the “drying out” of Mars, a general loss of clay minerals and other silicate and oxide minerals indicative of wetter conditions, to a drier sulfate-rich environment [6,7].

Hundreds of APXS measurements of the Mount Sharp group reflect the sulfate mineralogy, which was controlled primarily by Ca-sulfates until the transition into Mg-sulfate-bearing strata [31]. Figure 7 summarizes APXS data for sulfur, calcium, and magnesium throughout the strata discussed in this paper. Bearing in mind that Ca is present in plagioclase (predominantly andesine), and Ca and Mg are both present in Ca-pyroxene, two common detrital minerals, there is nevertheless an overprint of Ca:S correlation common throughout all sediments. In the Mg-sulfate-bearing unit, this correlation is offset to higher sulfur (Figure 7a) because of the addition of Mg-sulfates (Figure 7b). Figure 7a also shows that the Mg-sulfate-bearing unit has some local variability, where either Mg-sulfates or Ca-sulfates drive variation; this is illustrated by comparing the analyses from the Mineral King drill site (pink squares) in Figure 7a,b, where trends of enriched Mg-sulfate and Ca-sulfate are both found, radiating from a common central cluster. In summary, the transition into the Mg-sulfate-bearing unit marks a major shift to more abundant and more varied sulfates, but across this transition the common occurrence of gypsum, bassanite, and anhydrite has persisted.

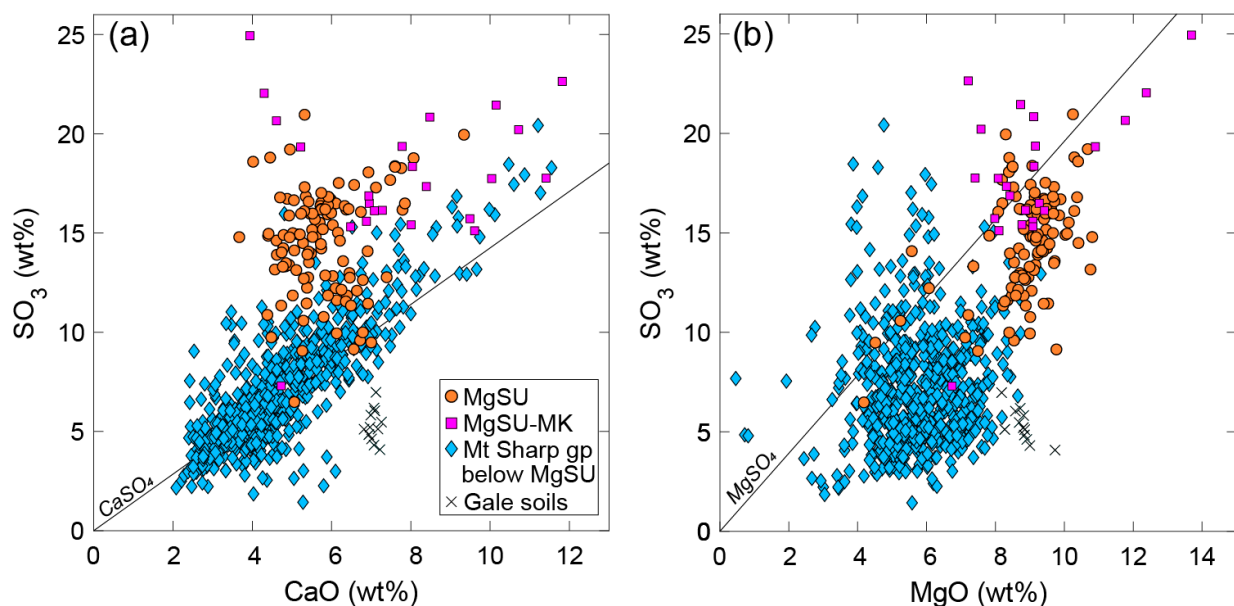


**Figure 7.** A summary of APXS analyses of  $\text{SO}_3$ , MgO, and CaO at Gale crater. Colored symbols separate the lower Mount Sharp group (blue diamonds) from the overlying Mg-sulfate-bearing unit (orange circles and pink squares). Regression lines show the  $\text{CaSO}_4$  trend in panel (a) and the  $\text{MgSO}_4$  trend in panel (b). Note that analyses in the vicinity of the sample Mineral King (MgSU-MK, pink squares) include analyses that parallel both Mg-sulfate (b) and Ca-sulfate (a) trends. Analyses of soils (X), distinct from the sediments, are shown for comparison.

### 3.2. A Sulfate Mineral Tour through Gale Crater Strata

Three intervals within the Mount Sharp group were singled out as targets of particular mineralogical interest during site selection [6]: (1) an erosionally resistant hematite-rich



interval (Vera Rubin Ridge); (2) a section immediately above that ridge with abundant clay minerals (Glen Torridon region); and (3) an upper transition into sediments with Mg-sulfate minerals (originally identified from orbit as kieserite and Mg-sulfates of higher hydration). The MSL mission is still in progress but, at the time of writing, has analyzed samples from all three of these intervals. These are treated below by stratigraphic position, which generally conforms to elevation ascending Mount Sharp. The discussion that follows is keyed to the sample locations in Figures 4 and 5.

The Pahrump Hills member of the Murray formation, consisting of mudstones, has the biggest gap in Ca-sulfate occurrence (Figure 5), with no detection in Confidence Hills and Mojave2 and only trace amounts of bassanite and anhydrite at Telegraph Peak. Coincident with the absence of Ca-sulfates is the presence of jarosite. In the lower Pahrump (Mojave2 and Confidence Hills), there are concretions and dendrites of Mg,Ni-sulfate associated with pseudomorphs that suggest replacement of prior Ca-sulfate [32,33]. Jarosite appears to have formed in a younger, possibly terminal alteration [34], the last act in a series of alteration events. Martin et al. [34] measured the K-Ar age for this jarosite as ~2.6 Ga; it is thus substantially younger than the inferred age of the Mt. Sharp group strata, which are constrained at ~3.6–3.2 Ga [35,36]. Jarosite occurs sporadically in the overlying portions of the Murray formation, where gypsum, bassanite, and anhydrite often occur together with the jarosite, allowing explanations other than acid-sulfate conditions for absence of Ca-sulfate (e.g., solutions below Ca-sulfate saturation) in the Pahrump Hills member or simply illustrating a limited amount and strength of acidic pH ([32] limits pH as >2). The Mojave2 sample was particularly informative because, although it lacks Ca-sulfate minerals, the drill site has abundant secondary rosettes of Mg,Ni-sulfate. The rosettes could not be sampled directly, but chemical analysis by the APXS [37,38] suggests a composition of  $\sim\text{Mg}_{0.9}\text{Ni}_{0.1}\text{SO}_4 \cdot n\text{H}_2\text{O}$ . Although drilling at Mojave2 did not target a rosette, the APXS analysis of the drill site shows that several percent of this material was in the drill sample delivered for XRD and would have been determined as an Mg-sulfate mineral if crystalline, indicating that it is instead X-ray amorphous. In general, the Pahrump Hills strata show evidence for abundant sediment-engulfing evaporite pseudomorphs and also include centimetric concretions along repeated horizons enriched in Mg-sulfate, as observed by ChemCam [39]. The Mojave2 sample provides an important contrast to Mg-sulfates of the stratigraphically higher Mg-sulfate-bearing unit, where APXS analyses show no comparable Ni association with sulfates, and Ca- and Mg-sulfate minerals commonly occur together.

The Buckskin sample near the top of the Pahrump Hills member deserves a brief mention. This sample is unique because the bulk composition is silica-rich (>80% SiO<sub>2</sub> [40]), represented in part by the unexpected low-pressure, high-temperature silica polymorph tridymite, which forms 14 wt% of the sample. The presence of tridymite suggests detritus from a silicic volcanic source [41,42], but a hydrothermal or fumarolic origin has also been proposed [43]. The only sulfate mineral in Buckskin is ~0.7% anhydrite.

Above the Pahrump member, the remainder of the Murray formation consists of mudstone and sandstone with variable Ca-sulfate content. Oudam was the first drill sample to contain gypsum, and gypsum is common to many samples throughout the upper Murray formation. Bassanite and anhydrite often occur together with gypsum, but the Oudam sample, which had gypsum but no bassanite, provided the critical evidence that a sample with only gypsum will produce bassanite by dehydration over several sols inside ChemMin. As mentioned above, in gypsum-bearing samples the first night of analysis represents the in situ Ca-sulfate mineral abundances. Jarosite, discussed above for the Pahrump Hills member, occurs sporadically throughout the rest of the Murray formation. Notably, throughout the Murray formation above Pahrump and below Vera Rubin Ridge, ChemCam identified host bedrock with intermittent centimetric horizons containing 30 to 50 wt.% Ca-sulfate enrichments [23]. These disseminated Ca-sulfates, forming intra-sediment salt deposits, are intertwined with thicker host bedrock intervals devoid of sulfates. The hydration of these intra-sediment Ca-sulfates seems consistent with

a mixture of both bassanite and anhydrite (Figure 6), but the distinction of the two using elemental stoichiometry is rendered difficult by fine-scale dilution within the bedrock.

From Aberlady through Glasgow, across the contact between the Murray formation and the Carolyn Shoemaker formation of the Glen Torridon region, the sediments contain abundant clay minerals (19% to 30%). Within this stratigraphic sequence is the erosionally resistant Vera Rubin Ridge, represented by the samples Duluth, Stoer, Highfield, and Rock Hall [44]. Vera Rubin Ridge is a complex diagenetic zone where alteration to, and deposition of, crystalline hematite was concentrated, making the sediments more resistant to erosion [44–46]. The fracture-fill materials are predominantly Ca-sulfate but have distinct variability with Fe-enrichments, highlighting the interactions of fracture fluids with their host bedrock [47]. Within the Glen Torridon, bassanite and anhydrite are common, but gypsum is almost absent. The sole sample containing gypsum is Highfield, on Vera Rubin Ridge. Highfield needs to be considered in relation to the nearby sample Rock Hall (~35 m distant and ~3 m higher). These two samples were targeted specifically because they have two spectrally different forms of hematite alteration, gray (Highfield) and red (Rock Hall). Together they represent the Jura formation, the uppermost, resistant spine of Vera Rubin Ridge. Left begging is the question of why Highfield has gypsum when Rock Hall, and all other samples from Aberlady to Glasgow, do not. A clue may be in the difference between the red and gray lithologies. The gypsum-bearing gray sample at Highfield is indeed hematite-rich (9.3%); the gypsum-absent red sample at Rock Hall has a comparable abundance of total Fe-oxide but as a mixture of hematite (2.9%) and akaganeite (6%). Akaganeite formation is favored in acidic saline solutions, and [45] suggests that the absence of gypsum and dominance of anhydrite in Rock Hall may be a marker of either (1) longer-lived aqueous activity to allow for transition of gypsum and/or bassanite to anhydrite, (2) an open hydrologic system in the presence of saline fluids, or (3) slightly elevated temperatures  $> \sim 60$  °C. The gypsum at Highfield would form from solutions that differ from these conditions. Alternatively, the drill site at Highfield is laced with a dense network of fine light-toned veins that may represent a later, localized diagenetic system that precipitated gypsum.

In the rest of the Glen Torridon and Vera Rubin Ridge, although gypsum is absent, bassanite and anhydrite are abundant as diagenetic features [48]. Bristow et al. [5] cite a 9.22 Å structure as evidence of a mixed-layer serpentine–talc component in smectite of the Glen Torridon and suggest that silica-poor, sulfate-dominated brines, potentially sourced during deposition of the overlying Mg-sulfate-bearing unit, infiltrated to convert ferric smectites and ferrous-substituted serpentine–talc of the clay minerals into the iron oxides and oxyhydroxides of Vera Rubin Ridge. However, experiments with smectites, palagonites, and zeolites exposed to pure Mg-sulfate brine show that even small amounts of Ca in these phases will exchange for Mg in solution, leading to early precipitation of gypsum before Mg-sulfates [49]. At low temperatures ( $< \sim 50$  °C), Mg-rich brine infiltrating the Glen Torridon sediments should have produced gypsum. Thus, another factor in the absence of gypsum may be modestly elevated temperatures that are implicated in the clay mineralogy of the Glen Torridon [46], possibly in the range of 50–100 °C [50], where precipitation of anhydrite rather than gypsum or alteration of prior gypsum to anhydrite would occur. Bassanite generally forms by dehydration of gypsum (e.g., [51]), suggesting an origin separate from that of anhydrite. It is possible that earlier gypsum in the Glen Torridon dehydrated to bassanite as anhydrite was formed.

In the Mount Sharp group above the Glen Torridon, from Nontron to Pontours, mudstones rich in clay minerals are less common, and sulfate-enriched nodules become abundant. They are mostly present as Mg-sulfates but also as Ca-sulfates, and some are even organized in centimetric polygons interpreted as preserved columnar soil [52]. Above Pontours, in the Mirador formation, clay minerals are absent. Here, cross-stratified eolian sediments are abundant, with lesser intervals of thinly bedded sediments that likely represent interdune aqueous deposits. Gypsum, absent in the Glen Torridon, is once again common (along with bassanite and anhydrite). The Zechstein sample of a shallow

subhorizontal gypsum vein, discussed above with Figure 3, is within the eolian sediments of the Mirador formation.

A major transition in sulfate mineralogy occurs at Canaima, where the rover entered the Mg-sulfate-bearing unit that was a major stratigraphic target for the MSL mission. Canaima provided the first XRD confirmation on Mars of a polyhydrated Mg-sulfate mineral, starkeyite ( $\text{MgSO}_4 \cdot 4\text{H}_2\text{O}$ , [9]). Tapo Caparo, the next sample after Canaima, contained the monohydrated Mg-sulfate mineral kieserite ( $\text{MgSO}_4 \cdot \text{H}_2\text{O}$ ). Tapo Caparo was collected above a prominent “marker band” with ripple evidence of standing shallow water [53]. This marker band is a significant sedimentary horizon traceable around Mount Sharp [6,54]. From Tapo Caparo upward, the host sediment has both planar bedding and low-angle cross-bedding.

The detection of both starkeyite and kieserite matches the expectations for the Mg-sulfate-bearing unit laid out by remote sensing before the MSL mission [6]. The significance of the Mg-sulfates starkeyite and kieserite is related to a transition to more sulfate-rich sediments, as seen in Figures 6 and 7. These two minerals have so far been found consistently in drill samples of the Mg-sulfate-bearing unit but appear to be mutually exclusive. The exploration of this unit is continuing. A key finding from the sulfate unit is the association of not only Ca- and Mg-sulfate salts but also significant abundances (5 to 11 wt%) of the Fe-carbonate siderite above the marker band (from Tapo Caparo upward). The unexpectedly high abundances of siderite indicate that it had an active role in the Martian carbon cycle when the layered sulfate unit was forming [55]. These samples also confirm the continuity of gypsum, bassanite, and anhydrite occurrences throughout the Bradbury and Mount Sharp sequence across the transition to Mg-sulfate and Fe-carbonate appearance.

Above the Bradbury–Mount Sharp groups, the unconformably overlying Stimson formation remains poorly known, and of the five samples analyzed, two are heavily altered vein walls. Aside from the intensive wall-rock alteration, differences in the Stimson are evident between the samples at the two locations that were drilled: bassanite–anhydrite without clay minerals at the Naukluft Plateau (Okoruso and Big Sky) and clay minerals with no sulfate minerals at Siccar Point (Edinburgh). The pre-alteration detrital mineralogy also differs, with no olivine at the Naukluft Plateau (lost to alteration?) yet abundant olivine at Siccar Point. Later attempts to cross the unconformity into the Stimson found a hardened and angular terrain that was too hazardous for the rover to traverse and too difficult or too hard to drill (Figure 2).

Finally, modern eolian samples at Gale crater (Rocknest, Gobabeb, and Ogunquit Beach) provide a view of sulfate mineralogy in recent un lithified basaltic sands of Mars. Here, gypsum is absent, and the sole sulfate mineral detected is a small amount of anhydrite (~1% in all scooped sand samples). Differential abrasion and loss of softer gypsum and bassanite may be a factor in the absence of gypsum and bassanite, but other processes can occur. Vaniman et al. [10] cite several localities on Earth where gypsum in a dry environment is reported to transform first to bassanite and ultimately to anhydrite. For one well-documented example, Moiola and Glover [56] used optical petrography and XRD to study gypsum at Clayton Playa in Nevada, USA, where initial wet growth of cm-scale gypsum crystals followed by surface exposure produces a thin (~60  $\mu\text{m}$ ) layer of bassanite between the gypsum core and an outer layer (~500  $\mu\text{m}$ ) of anhydrite, supporting an interpretation of progressive desiccation from the gypsum core to the anhydrite rim. Vaniman et al. [10] suggest that a similar transformation of gypsum to anhydrite may occur with millennia of exposure and eolian cycling of dark basaltic sands that can reach relatively high summer temperatures on Mars.

#### 4. Broader Considerations

##### 4.1. Gypsum and Other Ca-Sulfates at Gale Crater Are Persistent through Strata and Time

Figure 5 shows that gypsum, bassanite, and anhydrite are common through the sequence of the Bradbury and Mount Sharp group sediments at Gale crater. This through-going occurrence of Ca-sulfates contrasts markedly with the more restricted stratigraphic

distribution of jarosite and the Mg-sulfates. Absences of any Ca-sulfates in drill samples are few, and only in the basal Pahrump member (Confidence Hills and Mojave2), but even there a petrographic assessment of crystal pseudomorphs suggests that gypsum was once present [33]. This persistence in space is likely matched by persistence over time, considering the evidence of later veins mostly composed of gypsum (Zechstein, [17]) and drill samples of veins cross-cutting the unconformity beneath the Stimson formation (Lubango and Greenhorn, [57]) that include gypsum, bassanite, and anhydrite.

In the bulk of the Stimson formation, the total sulfate mineral abundances are small (<2% bassanite and anhydrite, no gypsum) in samples away from the Lubango and Greenhorn vein alteration. The Edinburgh sample of the Stimson has no sulfate minerals. Moreover, as discussed above, modern eolian sands also contain only minor (~1%) anhydrite and no other sulfate minerals. These results could suggest that contributions of sulfate minerals at Gale crater diminished as the Martian environment became drier, although the small number of Stimson and modern eolian samples makes this conjecture speculative. As the MSL mission progresses, the rover will be traversing through strata where sulfate spectral signatures weaken [6]; mineralogical analyses of these upper strata will provide more data on the younger sulfate history.

#### 4.2. Gypsum Is at the Edge of Stability near the Martian Equator

Figure 3, showing the progressive dehydration of gypsum to bassanite in the Zechstein sample at moderately elevated temperature, reinforces the conclusions of [10] that above the minimum drill sample depth (i.e., at >2 cm depth), gypsum can transform to bassanite in Mars equatorial conditions. This conclusion is further supported by the lack of evidence for hydration higher than bassanite in ChemCam laser ablation analyses of surface-exposed Ca-sulfates at Gale crater [16]. *Curiosity's* younger sister rover *Perseverance*, with the Mars 2020 mission at Jezero crater, is also at a near-equatorial site and has encountered common surface occurrences of low-hydration Ca-sulfates (anhydrite and bassanite) but, so far, very little gypsum [58,59]. Surface-exposed gypsum has also been reported by orbital spectroscopy in the near-equatorial layered deposits associated with Valles Marineris (e.g., [60]), but the spectral identification of gypsum there has been questioned [7].

Even at low latitudes, gypsum may still be preserved at the surface if conditions are favorable. As noted above, surface temperatures that can rise above a few degrees centigrade, exposure to desiccating winds, and prolonged exposure through slow erosion rates are likely requirements for the dehydration of gypsum. Some evidence of surface gypsum is found at Gale crater, indicated by Mastcam near-IR spectral filters sensitive to hydration in veins of the Bradbury group that were not sampled, near Cumberland and John Klein ([25] supplement). At another near-equatorial site, encountered by the MER rover *Opportunity* (MER-B in Figure 1) on the rim of Endeavor crater, a gypsum vein was identified based on spectra [61]. The near-equatorial survivability of surface-exposed gypsum may be affected by crystal size, crystal habit, rock fabric, and other petrologic factors; Vaniman et al. [10] show that gypsum in a range of rock fabrics has dehydration rates an order of magnitude slower than in silt- to sand-size grains and that denser rock fabrics (e.g., nodular evaporite) dehydrate at rates an additional order of magnitude slower than porous fabrics (satin spar). Under the right conditions, gypsum can survive on surfaces exposed at low latitudes.

#### 4.3. Gypsum Is More Stable and More Abundant at Higher Latitudes

Temperatures on the Martian surface are cold enough at higher latitudes that lander and rover operations are challenging, so most surface exploration has been at lower latitudes. A major exception was the 2008 Phoenix mission, which landed at ~68° north latitude. The Phoenix lander was not equipped with an instrument to determine mineralogy, but it did have a Wet Chemistry Laboratory (WCL) that used a leaching solution and ion-selective electrodes to determine ionic species, pH, and the electrical conductivity of soluble salts in regolith scooped at the site. Analyses by the WCL revealed significant



amounts of soluble sulfate salts, charge-balanced by Mg and Ca cations with  $Mg > Ca$ ; modeling suggests that gypsum and epsomite (and perhaps meridianiite) were present as salts in the regolith [62].

The Phoenix lander pushed the envelope on Mars landings by going to such a high latitude, but it was still at a latitude ~700 km south of the largest gypsum deposit yet known on Mars, in the Olympia Undae sand sea [63]. Olympia Undae is part of an extensive circumpolar dune field that covers 844,000 km<sup>2</sup> [64]. At Olympia Undae, the spectral signature of gypsum is dominant, though recent analyses have also identified bassanite [65]. This gypsum-rich sand sea has both transverse and barchan dune forms that reveal katabatic wind patterns originating from the north polar ice cap. Despite abundant gypsum, which should be light in color if inclusion-free, the dune field is among the darkest sand deposits on Mars. The dark color may be attributed to pyroxene-rich sand [63] and other mafic minerals. Several possible origins for the gypsum have been proposed, including an influx of polar meltwater and the precipitation of gypsum from pore fluids, with sulfur and cations derived from alteration of high-Ca pyroxene and sulfide sand grains [63]; cementation of mafic sands by a water table rise of solutions, with sulfate derived from both sulfide weathering and atmospheric input [66]; and eolian weathering and transport of both gypsum and mafic minerals from the margins of a sedimentary unit beneath the polar ice cap [64].

The vast extent of the gypsum-bearing polar dunes puts them in a class beyond what has been observed at Gale crater and other gypsum occurrences at lower latitudes. Another distinction from lower latitudes is the very young age of the polar dune field. The polar sand sea is extremely well preserved, and despite the vast area covered it has only one significant impact crater, which places it in the Martian timescale of “late Amazonian”, or younger than ~400 Ma [63]. This young age contrasts markedly with the much older age of sediments and sulfates at Gale crater, where crater formation is estimated at ~3.6 Ga [35] and sediment infilling up to ~3.2 Ga [36]. Mineral-forming events persisted much later, with a SAM instrument K/Ar age of jarosite at Mojave2 indicating some sulfate precipitation <3 Ga, possibly as late as ~2.6 Ga [34].

As mentioned in the introduction, Gale crater is on the dichotomy boundary that separates the ancient highlands of the southern hemisphere from the northern lowlands on Mars. The northern lowlands present a little-cratered and much younger surface that is the sink for several fluvial channel systems sourced from the south. Some papers suggest that a significant body of water once existed in the northern hemisphere [67]. If so, the lowland could host evaporite salt bodies, including massive gypsum, more similar to Earth than the small percentages of Ca-sulfate that occur as cement in clastic sediments or as later fracture fills at Gale crater.

#### 4.4. Gypsum and the Water Inventory of Mars

Ideal gypsum has a water content of 20.9 wt%. When found in abundance, gypsum can be a significant reservoir of mineral-bound water. Feldman et al. [68] used Mars Odyssey Neutron Spectrometer (MONS) data to map global “water-equivalent hydrogen” (WEH), which includes contributions of not just ice but also water and structural OH in hydrous minerals. The MONS neutron data are not of the exposed surface but, as with the Mars Odyssey GRS map of sulfur (Figure 1), come from depths as great as ~1 m, where the activity of water can be considerably higher than at the surface. In permafrost regions above ~50° latitude it is certain that pore ice is present, but modeling allows for hydrous salts as well. As examples, [69] cites kieserite ( $MgSO_4 \cdot H_2O$ ; 13 wt%  $H_2O$ ) or lesser amounts of hexahydrite ( $MgSO_4 \cdot 6H_2O$ ; 47 wt%  $H_2O$ ) as possible phases to account for much of the WEH observed. Gypsum is certainly another possibility, especially given the known occurrence of gypsum intimately associated with ice near the north pole.

At Gale crater, where permafrost is absent, WEH in hydrous minerals can be examined in detail from XRD data. Using the average percentage mineral contents of the Mount Sharp group below the layered sulfate unit, the average gypsum content of 3 wt% accounts

for only 0.6 wt% water in the bulk rock, though unsampled fracture gypsum, as found at Zechstein, would increase this amount, perhaps to several percent in rock intensely laced by gypsum in fractures. In comparison, the 17 wt% average abundance of clay minerals could account for considerably more water. Structural OH in these smectitic clays is ~4 wt% of the mineral; this OH alone accounts for 0.7 wt% water equivalent in the bulk rock. Moreover, although the clay minerals analyzed by CheMin are mostly collapsed with little interlayer water, they are capable of significant interlayer water content at depths where humidity is higher [70]. At high humidity, in vapor communication with ice, a typical smectite can hold ~25 wt% interlayer water [71]. This capability would account for >4 wt% water in the bulk average of the Mount Sharp group. Only extensive bedded gypsum deposits, not found so far on Mars, could match the water-bearing capacity of deposits rich in clay minerals of ice-bearing sediments at depth.

Where clay minerals are absent, as in the Mg-sulfate-bearing unit, starkeyite ( $\text{MgSO}_4 \cdot 4\text{H}_2\text{O}$ ; 37 wt%  $\text{H}_2\text{O}$ ) has so far been the most hydrated salt. Kieserite ( $\text{MgSO}_4 \cdot \text{H}_2\text{O}$ ; 13 wt%  $\text{H}_2\text{O}$ ) is a lesser contributor to hydration. The sample at Ubajara has 6 wt% starkeyite, representing 2.2 wt% water in that sample, but starkeyite is not always present. In the 500 m of the Mg-sulfate unit sampled so far, the average abundance of starkeyite is ~2 wt%, but the number of samples on which this estimate is based is small. Gypsum has persisted at a current average of ~1 wt% throughout the Mg-sulfate-bearing unit, so it remains a contributor to water inventory. Gypsum may be more important than this small percentage would suggest if fracture fills were included; fracture fills are known to contain gypsum but not starkeyite or other Mg-bearing sulfates. A future target of MSL is a set of large-scale mineral-filled fractures in a feature known as the “boxwork”, higher in Gale crater stratigraphy, where a swarm of massive, meter-scale fractures covers an area of ~0.35 km<sup>2</sup> [72]. The mineral fillings of these fractures cannot be determined from orbital observations, but sulfates are expected, and gypsum is a potential candidate.

An important unknown in water inventory is the hydration state for the ~40 wt% X-ray amorphous material found in all CheMin samples. The SAM evolved gas analysis data show that, for most samples, ~1 to 3 wt% water is released on heating to 800 °C [73], which includes contributions from both the amorphous component and all hydrous minerals. Opal-CT has also been confirmed by XRD in several samples, but opal-A without characteristic diffraction is also present in specific occurrences; both may contain some water [74] but distinguishing opal-A from overall amorphous diffraction is problematic [41]. Perhaps half of the water release can be attributed to the amorphous component in some samples, but certainly not an overwhelming amount. The most significant unknown in the possible hydration of the amorphous material is the extent to which amorphous material may accumulate water at depths where humidity can be higher, particularly if the X-ray amorphous material includes hygroscopic or protoclay components.

#### 4.5. Gypsum and Associated Sulfate Origins at Gale Crater

Mars is a sulfur-rich planet throughout, from the core to the surface, and the sulfur cycle on Mars may be the most important geochemical cycle on the planet [75]. Sulfur residing in the crust (Figure 1) was derived through several processes, including degassing, magmatism, hydrothermal activity, and impact processes at a wide range of energies. The detailed data on gypsum and other sulfate minerals from Gale crater provide some site-specific constraints on formation, but Mars is a complex planet and divergence from what has been found at Gale is seen in evidence for other sulfate minerals, notably Fe-sulfates such as szomolnokite [76], not found at Gale crater.

In sulfate mineralogy, what has been found at Gale crater are widespread occurrences of Ca-sulfates (gypsum, bassanite, anhydrite), dispersed occurrences of jarosite, and the appearance of the Mg-sulfates starkeyite and kieserite in younger sulfate-rich sediments above the last significant occurrences of clay minerals. The most obvious occurrence of Ca-sulfate is that which fills late fractures that pervasively cross-cut sedimentary strata throughout the entire Mt. Sharp group and Siccar Point group succession. Otherwise, of

the many possible ways of forming sulfate minerals in the sedimentary rock record of Mars [7], there are some that can be discounted at Gale crater. There is a notable lack of stratified gypsum or other thick sulfate evaporite deposits that are common in terrestrial evaporite systems. Sulfate minerals found in the 43 XRD analyses at Gale crater account for 20% or less of the bulk rock (Figure 5; and <13% if the gypsum vein at Zechstein is discounted). No concentrated, bedded evaporite deposits dominated by salts are found. Evaporation processes may still impact salt formation, as in cyclical surface wetting and drying reported by [52], but discrete evaporite beds do not occur. Importantly, other salts typically associated in massive salt assemblages are generally lacking; we want to point out, however, that though halite occurrences have been rare, the latest sample, Mineral King, has the most halite yet found (4.3%—as much as the total other salts, anhydrite and kieserite, in this sample). As the MSL mission progresses up-section, our view of salt origins may evolve. So far, however, the evidence at Gale shows that the common mode of sulfate mineral occurrence is either as dispersed salts that fill matrix pores of sedimentary rocks or at higher concentrations within fractures. Fracture transport and deposition of salts within groundwater systems has clearly been a significant process at Gale crater.

Large sulfur isotope fractionations in the sediments of Gale crater support models of an active fluvio-lacustrine system modified by later diagenesis in which sulfur, sulfites, and sulfides oxidized to sulfate in multiple diagenetic events [77]. Studies of clay mineral alteration [78] and hypotheses for Mg-sulfate formation [79] point to significant brine migration within the sediments of Gale crater. However, later diagenetic events may not have led to the complete dissolution and re-equilibration of earlier-formed salt mineralogy. For example, notable in the Ca-sulfates of Gale crater, and in contrast to systems familiar on Earth, is the metastable association of multiple hydration states with gypsum, bassanite, and anhydrite, commonly occurring together. On a wetter and warmer planet such as Earth, conversion entirely to either gypsum or anhydrite, with the loss of bassanite intermediates, is the norm. Even in the “wetter” environment of clay minerals below the Mg-sulfate-bearing unit, the lower temperatures and low activity of water on Mars have been insufficient to drive these associations to equilibrium.

Finally, as discussed in Section 3.2, the jarosite of the Pahrump member at Gale crater was formed at a very late stage, ~2.6 Ga [34,80], considering the much earlier date of the Gale crater impact (~3.6 Ga, [35]). The implication of this is that these salts, formed at higher acidity, may have formed late in the history of the Gale sedimentary basin. The tremendous age range from 3.6 to 2.6 Ga allows at least  $10^9$  years of sedimentary and alteration history. The impact generation of the crater led to a relatively brief but thermally intense period of hydrothermal activity [81],  $\sim 3 \times 10^5$  years; although this is <0.1% of the period from 3.6 to 2.6 Ga, the hydrothermal dissipation of impact superheat undoubtedly had a significant impact on the sulfate system. Some sulfur was lost by impact vaporization, but fallback and hydrothermal activity involving the melt sheet and surrounding crust will have replenished the sulfate system. Modeling suggests significant amounts of anhydrite formed [81], which may have provided a source of Ca-sulfate for much younger fracture systems. Following this relatively brief episode, fluvio-lacustrine systems transitioning to greater eolian activity persisted up to and beyond the ~2.6 Ga formation of jarosite [35]. The combined history of sedimentation and especially of later alteration at Gale crater represents a timespan on the scale of the entire Phanerozoic on Earth. That is plenty of time for a multitude of processes to play out.

#### 4.6. Gypsum and the Future Exploration of Mars

The detailed mineralogy from Gale crater shows that gypsum is widely encountered in sediments dating from early, wet Mars, as well as in later sediments formed as the planet evolved to dryer environments. Remote sensing studies of the much younger, polar gypsum deposits indicate that gypsum has played a significant role throughout the planet's history. These “end-member” locations, equatorial and polar, reveal the very broad range of settings where gypsum occurs on Mars. Future missions are certain to encounter gypsum

again in settings and associations already known but likely also in unexpected ways. There are several reasons to incorporate gypsum studies into Mars exploration goals. Expanded knowledge of the history of water on Mars is a primary reason. Other reasons hinge on gypsum's water content, both as a potential resource (if present in sufficient quantity) and as a marker of potentially habitable systems (as long as salinity does not become too high, [82]).

Studies of gypsum on Earth at several “planetary analog” locations have addressed gypsum as a possible host for life on Mars. For example, [83] studied gypsum in salars of the Chilean Andes and found a variety of microorganisms, both entrapped in the mineral host and as potentially viable prokaryotes and eukaryotes within fluid inclusions. Similarly, [84] found that hydrothermal gypsum deposits in the Haughton impact structure on Devon Island in Canada have viable cyanobacteria along cleavage planes within gypsum crystals. Notably, the photosynthetic cyanobacteria have adapted to survival within transparent selenite crystals by dissolution and expansion of cleavage planes to ~1 mm and by development of dark pigments that screen harmful UV radiation. Perhaps most exciting in these studies is the potential for extant life cocooned in a “tailored” environment of fluid inclusion refugia. If life adapted to fluid inclusions is to be sought, gypsum and halite (halite recently found at 4.3 wt% in the Gale crater sample Mineral King) are the likeliest hosts on Mars, with gypsum the most abundant.

**Author Contributions:** Investigation, all authors; methodology, D.V., S.C., E.R., T.B., D.B., J.M., T.P., D.M., P.C., N.C., R.T.D., S.M., R.H., R.M., A.P., A.H.T., A.Y., C.A., B.T., E.H., S.S., M.T., V.T., D.J.D.M. and J.G.; data collection, D.V., S.C., E.R., T.B., D.B., J.M., W.R., J.B., D.M., P.C., N.C., R.T.D., S.M., R.H., R.M., A.P., A.H.T., A.Y., C.A., B.T., E.H., S.S., M.T., V.T. and D.J.D.M.; data analysis, D.V., S.C., E.R., T.B., D.B., J.M., T.P., W.R., J.B., D.M., P.C., N.C., R.T.D., S.M., R.H., R.M., A.P., A.H.T., A.Y., C.A., B.T., E.H., S.S., M.T., V.T. and D.J.D.M.; figure production, D.V., W.R., J.B. and A.F.; writing—original draft preparation, D.V.; management, T.B., E.R. and A.F. All authors have read and agreed to the published version of the manuscript.

**Funding:** Funding for this work came from NASA's Mars Exploration Program through the Mars Science Laboratory project via the contributors' respective instrument PIs and the MSL Participating Scientist Program. A portion of this research was carried out at the Jet Propulsion Laboratory, California Institute of Technology, under a contract with the National Aeronautics and Space Administration (80NM0018D0004).

**Data Availability Statement:** Publicly available datasets were analyzed in this study. These data can be found here: <https://pds.nasa.gov>, accessed on 26 June 2024. Additional contextual information can be found in the publicly available Gale crater Mineralogy and Geochemistry Sample Database found here: <https://doi.org/10.48484/JN48-YW52> (accessed on 20 June 2024) and the CheMin Database (<https://odr.io/CheMin#/search/display/84/eyJkdF9pZCI6JmZlZm91I>) (accessed on 20 June 2024).

**Acknowledgments:** The authors are grateful to Suniti Karunatillake of Louisiana State University for discussions of the 2001 Mars Odyssey mission orbital gamma ray spectrometer (GRS) data shown in Figure 1. We would also like to acknowledge the very helpful corrections and suggestions offered by three anonymous reviewers.

**Conflicts of Interest:** The authors declare no conflicts of interest.

## References

1. Bibring, J.-P.; Langevin, Y.; Gendrin, A.; Gondet, B.; Poulet, F.; Berthé, M.; Soufflot, A.; Arvidson, R.; Mangold, N.; Mustard, J.; et al. Mars surface diversity as revealed by the OMEGA/Mars Express observations. *Science* **2005**, *307*, 1576–1581. [[CrossRef](#)] [[PubMed](#)]
2. Murchie, S.; Arvidson, R.; Bedini, P.; Beisser, K.; Bibring, J.-P.; Bishop, J.; Boldt, J.; Cavender, P.; Choo, T.; Clancy, R.T.; et al. Compact Reconnaissance Imaging Spectrometer for Mars (CRISM) on Mars Reconnaissance Orbiter (MRO). *J. Geophys. Res. Planets* **2007**, *112*, E05S03. [[CrossRef](#)]
3. Jamieson, C.S.; Noe Dobra, E.Z.; Dalton III, J.B.; Pitman, K.M.; Abbey, W.J. The spectral variability of kieserite (MgSO<sub>4</sub>·H<sub>2</sub>O) with temperature and grain size and its application to the Martian surface. *J. Geophys. Res. Planets* **2014**, *119*, 1218–1237. [[CrossRef](#)]



4. Wray, J.J.; Squyres, S.W.; Roach, L.H.; Bishop, J.; Mustard, J.F.; Noe Dobrea, E.Z. Identification of the Ca-sulfate bassanite in Mawrth Vallis, Mars. *Icarus* **2010**, *209*, 416–421. [[CrossRef](#)]
5. Karunatillake, S.; Wray, J.J.; Gasnault, O.; McLennan, S.M.; Rogers, A.D.; Squyres, S.W.; Boynton, W.V.; Skok, J.R.; Ojha, L.; Olsen, N. Sulfates hydrating bulk soil in the Martian low and middle latitudes. *Geophys. Res. Lett.* **2014**, *41*, 7987–7996. [[CrossRef](#)]
6. Milliken, R.E.; Grotzinger, J.P.; Thompson, B.J. Paleoclimate of Mars as captured by the stratigraphic record in Gale Crater. *Geophys. Res. Lett.* **2010**, *37*, 4. [[CrossRef](#)]
7. Grotzinger, J.P.; Milliken, R.E. The sedimentary rock record of Mars: Distribution, origins, and global stratigraphy. In *Sedimentary Geology of Mars*; Society for Sedimentary Geology (SEPM): Claremore, OK, USA, 2012; Special Pub. No. 102; pp. 1–48, Print ISBN 978-1-56576-312-8, CD/DVD ISBN 978-1-56576-313-5.
8. Fraeman, A.A.; Ehlmann, B.L.; Arvidson, R.E.; Edwards, C.S.; Grotzinger, J.P.; Milliken, R.E.; Quinn, D.P.; Rice, M.S. The stratigraphy and evolution of lower Mount Sharp from spectral, morphological, and thermophysical orbital data sets. *J. Geophys. Res. Planets* **2016**, *121*, 1713–1736. [[CrossRef](#)] [[PubMed](#)]
9. Chipera, S.J.; Vaniman, D.T.; Rampe, E.B.; Bristow, T.F.; Martínez, G.; Tu, V.M.; Peretyazhko, T.S.; Yen, A.S.; Gellert, R.; Berger, J.A.; et al. Mineralogical investigation of Mg-sulfate at the Canaima drill site, Gale crater, Mars. *J. Geophys. Res. Planets* **2023**, *128*, e2023JE008041. [[CrossRef](#)]
10. Vaniman, D.T.; Martínez, G.M.; Rampe, E.B.; Bristow, T.F.; Blake, D.F.; Yen, A.S.; Ming, D.W.; Rapin, W.; Meslin, P.-Y.; Morookian, J.M.; et al. Gypsum, bassanite, and anhydrite at Gale crater, Mars. *Am. Min.* **2018**, *103*, 1011–1020. [[CrossRef](#)]
11. Blake, D.; Tu, V.; Bristow, T.; Rampe, E.; Vaniman, D.; Chipera, S.; Sarrazin, P.; Morrison, R.; Morrison, S.; Yen, A.; et al. The Chemistry and Mineralogy (CheMin) X-ray diffractometer on the MSL Curiosity rover: A decade of mineralogy from Gale crater, Mars. *Minerals* **2024**, *14*, 568. [[CrossRef](#)]
12. Morrison, S.M.; Downs, R.T.; Blake, D.F.; Vaniman, D.T.; Ming, D.W.; Hazen, R.M.; Treiman, A.H.; Achilles, C.N.; Yen, A.S.; Morris, R.V.; et al. Crystal chemistry of Martian minerals from Bradbury Landing through Naukluft Plateau, Gale crater, Mars. *Am. Min.* **2018**, *103*, 857–871. [[CrossRef](#)]
13. Morrison, S.M.; Blake, D.F.; Bristow, T.F.; Castle, N.; Chipera, S.J.; Craig, P.I.; Downs, R.T.; Eleish, E.; Hazen, R.M.; Meusburger, J.M.; et al. Expanded insights into Martian mineralogy: Updated analysis of Gale crater’s mineral composition via CheMin crystal chemical investigations. *Minerals* **2024**, *14*, 773. [[CrossRef](#)]
14. Chipera, S.J.; Bish, D.L. FULLPAT: A full-pattern quantitative analysis program for X-ray powder diffraction using measured and calculated patterns. *J. Appl. Cryst.* **2002**, *35*, 744–749. [[CrossRef](#)]
15. Anderson, R.C.; Jandura, L.; Okon, A.B.; Sunshine, D.; Roumeliotis, C.; Beegle, L.W.; Hurowitz, J.; Kennedy, B.; Limonadi, D.; McCloskey, S.; et al. Collecting samples in Gale crater, Mars; an overview of the Mars Science Laboratory Sample Acquisition, Sample Processing and Handling System. *Space Sci. Rev.* **2012**, *170*, 57–75. [[CrossRef](#)]
16. Rapin, W.; Meslin, P.-Y.; Maurice, S.; Vaniman, D.; Nachon, M.; Mangold, N.; Schröder, S.; Gasnault, O.; Forni, O.; Wiens, R.C.; et al. Hydration state of calcium sulfates in Gale crater, Mars: Identification of bassanite veins. *Earth Planet. Sci. Lett.* **2016**, *452*, 197–205. [[CrossRef](#)]
17. Vaniman, D.T.; Chipera, S.J.; Martínez, G.; Rapin, W.; Rampe, E.B.; Bristow, T.; Blake, D.F.; Meusberger, J.; Ming, D.W.; Downs, R.T.; et al. Near-surface dehydration of salt hydrates at Gale crater, Mars. In Proceedings of the 55th Lunar and Planetary Science Conference (LPSC 2024), Houston, TX, USA, 11–15 March 2024; Volume 55, abst. no. 1327.
18. Gellert, R.; Rieder, R.; Brückner, J.; Clark, B.C.; Dreibus, G.; Klingelhöfer, G.; Lugmair, G.; Ming, D.W.; Wänke, H.; Yen, A.; et al. Alpha Particle X-Ray Spectrometer (APXS): Results from Gusev crater and calibration report. *J. Geophys. Res.* **2006**, *111*, E02S05. [[CrossRef](#)]
19. Campbell, J.L.; Perrett, G.M.; Gellert, R.; Andrushenko, S.M.; Boyd, N.I.; Maxwell, J.A.; King, P.L.; Schofield, C.D. Calibration of the Mars Science Laboratory Alpha Particle X-ray Spectrometer. *Space Sci. Rev.* **2012**, *170*, 319–340. [[CrossRef](#)]
20. Maurice, S.; Clegg, S.M.; Wiens, R.C.; Gasnault, O.; Rapin, W.; Forni, O. ChemCam activities and discoveries during the nominal mission of the Mars Science Laboratory in Gale crater, Mars. *J. Anal. At. Spectrom.* **2016**, *31*, 863–889. [[CrossRef](#)]
21. Clegg, S.M.; Wiens, R.C.; Anderson, R.; Forni, O.; Frydenvang, J.; Lasue, J.; Maurice, S. Recalibration of the Mars Science Laboratory ChemCam instrument with an expanded geochemical database. *Spectrochim. Acta Part B At. Spectrosc.* **2017**, *129*, 64–85. [[CrossRef](#)]
22. Rapin, W.; Meslin, P.-Y.; Maurice, S.; Wiens, R.C.; Laporte, D.; Chauviré, B.; Thomas, N.H. Quantification of water content by laser induced breakdown spectroscopy on Mars. *Spectrochim. Acta Part B At. Spectrosc.* **2017**, *130*, 82–100. [[CrossRef](#)]
23. Rapin, W.; Ehlmann, B.L.; Dromart, G.; Schieber, J.; Thomas, N.H.; Fischer, W.W.; Vasavada, A.R. An interval of high salinity in ancient Gale crater lake on Mars. *Nat. Geosci.* **2019**, *12*, 889–895. [[CrossRef](#)]
24. Grotzinger, J.P.; Sumner, D.Y.; Kah, L.C.; Stack, K.; Gupta, S.; Edgar, L.; Rubin, D.; Lewis, K.; Schieber, J.; Mangold, N.; et al. A habitable fluvio-lacustrine environment at Yellowknife Bay, Gale crater, Mars. *Science* **2014**, *343*, 1242777. [[CrossRef](#)]
25. Vaniman, D.T.; Bish, D.L.; Ming, D.W.; Bristow, T.F.; Morris, R.V.; Blake, D.F.; Chipera, S.J.; Morrison, S.M.; Treiman, A.H.; Rampe, E.B.; et al. Mineralogy of a mudstone at Gale crater, Yellowknife Bay, Mars. *Science* **2014**, *343*, 1243480. [[CrossRef](#)] [[PubMed](#)]
26. Bish, D.L.; Blake, D.F.; Vaniman, D.T.; Chipera, S.J.; Morris, R.V.; Ming, D.W.; Treiman, A.H.; Sarrazin, P.; Morrison, S.M.; Downs, R.T.; et al. X-ray diffraction results from Mars Science Laboratory: Mineralogy of Rocknest at Gale crater. *Science* **2013**, *341*, 1238932. [[CrossRef](#)] [[PubMed](#)]

27. Achilles, C.N.; Downs, R.T.; Ming, D.W.; Rampe, E.B.; Morris, R.V.; Treiman, A.H.; Morrison, S.M.; Blake, D.F.; Vaniman, D.T.; Ewing, R.C.; et al. Mineralogy of an active eolian sediment from the Namib dune, Gale crater, Mars. *J. Geophys. Res. Planets* **2017**, *122*, 2344–2361. [[CrossRef](#)]
28. Rampe, E.B.; Lapotre, M.G.A.; Bristow, T.F.; Arvidson, R.E.; Morris, R.V.; Achilles, C.N.; Weitz, C.; Blake, D.F.; Ming, D.W.; Morrison, S.M.; et al. Sand mineralogy within the Bagnold Dunes, Gale crater, as observed in situ and from orbit. *Geophys. Res. Lett.* **2018**, *45*, 9488–9497. [[CrossRef](#)]
29. Treiman, A.H.; Bish, D.L.; Vaniman, D.T.; Chipera, S.J.; Blake, D.F.; Ming, D.W.; Morris, R.V.; Bristow, T.F.; Morrison, S.M.; Baker, M.B.; et al. Mineralogy, provenance, and diagenesis of a potassic basaltic sandstone on Mars: ChemMin X-ray diffraction of the Windjana sample (Kimberley area, Gale crater). *J. Geophys. Res. Planets* **2016**, *121*, 75–106. [[CrossRef](#)] [[PubMed](#)]
30. L’Haridon, J.; Mangold, N.; Meslin, P.-Y.; Johnson, J.R.; Rapin, W.; Forni, O.; Wiens, R.C. Chemical variability in mineralized veins observed by ChemCam on the lower slopes of Mount Sharp in Gale crater, Mars. *Icarus* **2018**, *311*, 69–86. [[CrossRef](#)]
31. Berger, J.A.; Gellert, R.; McCraig, M.A.; O’Connell-Cooper, C.D.; Spray, J.G.; Thompson, L.M.; VanBommel, S.J.; Yen, A.S.; Rampe, E.B.; Clark, J.V. Isochemical Characteristics of the Clay-Sulfate Transition in Gale Crater, Mars: APXS Results from Mont Mercou to the Marker Band Valley. In Proceedings of the 54th Lunar and Planetary Science Conference (LPSC 2023), Houston, TX, USA, 13–17 March 2023; Volume 54, abst. no. 1662.
32. Rampe, E.B.; Ming, D.W.; Blake, D.F.; Bristow, T.F.; Chipera, S.J.; Grotzinger, J.P.; Morris, R.V.; Morrison, S.M.; Vaniman, D.T.; Yen, A.S.; et al. Mineralogy of an ancient lacustrine mudstone succession from the Murray formation, Gale crater, Mars. *Earth Planet. Sci. Lett.* **2017**, *471*, 172–185. [[CrossRef](#)]
33. Kah, L.C.; Stack, K.M.; Eigenbrode, J.L.; Yingst, R.A.; Edgett, K.S. Syndepositional precipitation of calcium sulfate in Gale Crater, Mars. *Terra Nova* **2018**, *30*, 431–439. [[CrossRef](#)]
34. Martin, P.E.; Farley, K.A.; Baker, M.B.; Malespin, C.A.; Schwenzer, S.P.; Cohen, B.A.; Mahaffy, P.R.; McAdam, A.C.; Ming, D.W.; Vasconcelos, P.M.; et al. A two-Step K-Ar experiment on Mars: Dating the diagenetic formation of Jarosite from Amazonian groundwaters. *J. Geophys. Res. Planets* **2017**, *122*, 2803–2818. [[CrossRef](#)]
35. Le Deit, L.; Hauber, E.; Fueten, F.; Pondrelli, M.; Rossi, A.P.; Jaumann, R. Sequence of infilling events in Gale Crater, Mars: Results from morphology, stratigraphy, and mineralogy. *J. Geophys. Res. Planets* **2013**, *118*, 2439–2773. [[CrossRef](#)]
36. Grotzinger, J.P.; Gupta, S.; Malin, M.C.; Rubin, D.M.; Schieber, J.; Siebach, K.; Sumner, D.Y.; Stack, K.M.; Vasavada, A.R.; Arvidson, R.E.; et al. Deposition, exhumation, and paleoclimate of an ancient lake deposit, Gale crater, Mars. *Science* **2015**, *350*, aac7575. [[CrossRef](#)] [[PubMed](#)]
37. Gellert, R.; Berger, J.A.; Boyd, N.; Campbell, J.L.; Desouza, E.D.; Elliott, B.; Fisk, M.; Pavri, B.; Perrett, G.M.; Schmidt, M.; et al. Chemical evidence for an aqueous history at Pahrump, Gale crater, Mars, as seen by the APXS. In Proceedings of the 46th Lunar and Planetary Science Conference (LPSC 2015), Houston, TX, USA, 16–20 March 2015; Volume 46, abst. no. 1855.
38. VanBommel, S.J.; Gellert, R.; Berger, J.A.; Campbell, J.L.; Thompson, L.M.; Edgett, K.S.; McBride, M.J.; Minitti, M.E.; Pradlera, I.; Boyd, N.I. Deconvolution of distinct lithology chemistry through oversampling with the Mars Science Laboratory Alpha Particle X-Ray Spectrometer. *X-ray Spectrom.* **2016**, *45*, 155–161. [[CrossRef](#)]
39. Schieber, J.; Bohacs, K.M.; Coleman, M.; Bish, D.; Reed, M.H.; Thompson, L.; Rapin, W.; Zalami, Y. Mars is a mirror—Understanding the Pahrump Hills mudstones from a perspective of Earth analogues. *Sedimentology* **2022**, *69*, 2371–2435. [[CrossRef](#)]
40. Frydenvang, J.; Gasda, P.J.; Hurowitz, J.A.; Grotzinger, J.P.; Wiens, R.C.; Newsom, H.E.; Edgett, K.S.; Watkins, J.; Bridges, J.C.; Maurice, S.; et al. Diagenetic silica enrichment and late-stage groundwater activity in Gale crater, Mars. *Geophys. Res. Lett.* **2017**, *44*, 4716–4724. [[CrossRef](#)]
41. Morris, R.V.; Vaniman, D.T.; Blake, D.F.; Gellert, R.; Chipera, S.J.; Rampe, E.B.; Ming, D.W.; Morrison, S.M.; Downs, R.T.; Treiman, A.H.; et al. Silicic volcanism on Mars evidenced by tridymite in high-SiO<sub>2</sub> sedimentary rock at Gale crater. *Proc. Nat. Acad. Sci. USA* **2016**, *113*, 7071–7076. [[CrossRef](#)] [[PubMed](#)]
42. Payré, V.; Siebach, K.L.; Thorpe, M.T.; Antoshechkina, P.; Rampe, E.B. Tridymite in a lacustrine mudstone in Gale crater, Mars: Evidence for an explosive silicic eruption during the Hesperian. *Earth Planetary Sci. Lett.* **2022**, *594*, 117694. [[CrossRef](#)]
43. Yen, A.S.; Morris, R.V.; Ming, D.W.; Schwenzer, S.P.; Sutter, B.; Vaniman, D.T.; Treiman, A.H.; Gellert, R.; Achilles, C.N.; Berger, J.A.; et al. Formation of tridymite and evidence for a hydrothermal history at Gale crater, Mars. *J. Geophys. Res. Planets* **2021**, *126*, e2020JE006569. [[CrossRef](#)]
44. Fraeman, A.A.; Edgar, L.A.; Rampe, E.B.; Thompson, L.M.; Frydenvang, J.; Fedo, C.M.; Catalano, J.G.; Dietrich, W.E.; Gabriel, T.S.J.; Vasavada, A.R.; et al. Evidence for a diagenetic origin of Vera Rubin Ridge, Gale crater, Mars: Summary and synthesis of Curiosity’s exploration campaign. *J. Geophys. Res. Planets* **2020**, *125*, e2020JE006527. [[CrossRef](#)] [[PubMed](#)]
45. Rampe, E.B.; Bristow, T.F.; Morris, R.V.; Morrison, S.M.; Achilles, C.N.; Ming, D.W.; Vaniman, D.T.; Blake, D.F.; Tu, V.M.; Chipera, S.J.; et al. Mineralogy of Vera Rubin Ridge from the Mars Science Laboratory ChemMin instrument. *J. Geophys. Res. Planets* **2020**, *125*, e2019JE006306. [[CrossRef](#)]
46. Thorpe, M.T.; Bristow, T.F.; Rampe, E.B.; Tosca, N.J.; Grotzinger, J.P.; Bennett, K.A.; Achilles, C.N.; Blake, D.F.; Chipera, S.J.; Downs, G.; et al. Mars Science Laboratory ChemMin data from the Glen Torridon region and the significance of lake-groundwater interactions in interpreting mineralogy and sedimentary history. *J. Geophys. Res. Planets* **2022**, *127*, e2021JE007099. [[CrossRef](#)]
47. L’Haridon, J.; Mangold, N.; Fraeman, A.A.; Johnson, J.R.; Cousin, A.; Rapin, W.; Wiens, R.C. Iron mobility during diagenesis at Vera Rubin Ridge, Gale crater, Mars. *J. Geophys. Res. Planets* **2020**, *125*, e2019JE006299. [[CrossRef](#)]

48. Gasda, P.J.; Comellas, J.; Essunfeld, A.; Das, D.; Bryk, A.B.; Dehouck, E.; Schwenzer, S.P.; Crossey, L.; Herkenhoff, K.; Johnson, J.R.; et al. Overview of the morphology and chemistry of diagenetic features in the clay-rich Glen Torridon unit of Gale crater, Mars. *J. Geophys. Res. Planets* **2022**, *127*, e2021JE007097. [[CrossRef](#)]
49. Vaniman, D.T.; Chipera, S.J. Transformations of Mg- and Ca-sulfate hydrates in Mars regolith. *Am. Min.* **2006**, *91*, 1628–1642. [[CrossRef](#)]
50. Turner, S.M.R.; Schwenzer, S.P.; Bridges, J.C.; Rampe, E.B.; Bedford, C.C.; Achilles, C.N. Early diagenesis at and below Vera Rubin Ridge, Gale crater, Mars. *Meteoritics Planet. Sci.* **2021**, *56*, 1905–1932. [[CrossRef](#)]
51. Mees, F.; De Dapper, M. Vertical variations in bassanite distribution patterns in near-surface sediments, southern Egypt. *Sed. Geol.* **2005**, *181*, 225–229. [[CrossRef](#)]
52. Rapin, W.; Dromart, G.; Clark, B.C.; Schieber, J.; Kite, E.S.; Kah, L.C.; Thompson, L.M.; Gasnault, O.; Lasue, J.; Meslin, P.-Y.; et al. Sustained wet–dry cycling on early Mars. *Nature* **2023**, *620*, 299–302. [[CrossRef](#)] [[PubMed](#)]
53. Weitz, C.M.; Lewis, K.W.; Kite, W.S.; Dietrich, W.E.; Thompson, L.M.; O’Connell-Cooper, C.D.; Schieber, J.; Rubin, D.; Gasda, P.; Mondro, C.; et al. The Marker Band in Gale crater: A synthesis of orbital and ground observations. In Proceedings of the 54th Lunar and Planetary Science Conference (LPSC 2023), Houston, TX, USA, 13–17 March 2023; Volume 54, abst. no. 1560.
54. Weitz, C.M.; Lewis, K.W.; Bishop, J.L.; Thomson, B.J.; Arvidson, R.E.; Grant, J.A.; Seelos, K.D.; Ettenborough, I. Orbital observations of a marker horizon at Gale crater. *J. Geophys. Res. Planets* **2022**, *127*, e2022JE007211. [[CrossRef](#)]
55. Tutolo, B.M.; Hausrath, E.M.; Kite, E.S.; Rampe, E.B.; Bristow, T.F.; Downs, R.T.; Treiman, A.; Peretyazhko, T.S.; Thorpe, M.T.; Grotzinger, J.P.; et al. In situ evidence of an active carbon cycle on ancient Mars. *AGU Fall Meet. Abstr.* **2023**, *2023*, P43A-06.
56. Moiola, R.J.; Glover, E.D. Recent anhydrite from Clayton playa, Nevada. *Am. Min.* **1965**, *50*, 2063–2069.
57. Yen, A.S.; Ming, D.W.; Vaniman, D.T.; Gellert, R.; Blake, D.F.; Morris, R.V.; Morrison, S.M.; Bristow, T.F.; Chipera, S.J.; Edgett, K.S.; et al. Multiple stages of aqueous alteration along fractures in mudstone and sandstone strata in Gale Crater, Mars. *Earth Planet. Sci. Lett.* **2017**, *471*, 186–198. [[CrossRef](#)]
58. Siljeström, S.; Czaja, A.D.; Corpolongo, A.; Berger, E.L.; Li, A.Y.; Cardarelli, E.; Abbey, W.; Asher, S.A.; Beegle, L.W.; Benison, K.C.; et al. Evidence of sulfate-rich fluid alteration in Jezero crater floor, Mars. *J. Geophys. Res. Planets* **2024**, *129*, e2023JE007989. [[CrossRef](#)]
59. Lopez-Reyes, G.; Nachon, M.; Veneranda, M.; Beyssac, O.; Madariaga, J.M.; Manrique, J.A.; Clavé, E.; Ollila, A.; Castro, K.; Sharma, S.K.; et al. Anhydrite detections by Raman spectroscopy with SuperCam at the Jezero delta, Mars. In Proceedings of the 55th Lunar and Planetary Science Conference (LPSC 2024), Houston, TX, USA, 11–15 March 2024; Volume 55, abst. no. 1721.
60. Gendrin, A.; Mangold, N.; Bibring, J.-P.; Langevin, Y.; Gondet, B.; Poulet, F.; Bonello, G.; Quantin, C.; Mustard, J.F.; Arvidson, R.; et al. Sulfates in Martian layered terrains: The OMEGA/Mars Express view. *Science* **2005**, *307*, 1587–1591. [[CrossRef](#)] [[PubMed](#)]
61. Squyres, S.W.; Arvidson, R.E.; Bell, J.F., III; Calef, F., III; Clark, B.C.; Cohen, B.A.; Crumpler, L.A.; de Souza, P.A., Jr.; Farrand, W.H.; Gellert, R.; et al. Ancient impact and aqueous processes at Endeavour crater, Mars. *Science* **2012**, *336*, 570–576. [[CrossRef](#)] [[PubMed](#)]
62. Kounaves, S.P.; Hecht, M.H.; Kapit, J.; Quinn, R.C.; Catling, D.C.; Clark, B.C.; Ming, D.W.; Gospodinova, K.; Hredzak, P.; McElhoney, K.; et al. Soluble sulfate in the Martian soil at the Phoenix landing site. *Geophys. Res. Lett.* **2010**, *37*, L09201. [[CrossRef](#)]
63. Fishbaugh, K.E.; Poulet, F.; Chevrier, V.; Langevin, Y.; Bibring, J.-P. On the origin of gypsum in the Mars north polar region. *J. Geophys. Res.* **2007**, *112*, E07002. [[CrossRef](#)]
64. Massé, M.; Bourgeois, O.; Le Mouélic, S.; Verpoorter, C.; Spiga, A.; Le Deit, L. Wide distribution and glacial origin of polar gypsum on Mars. *Earth Planet. Sci. Lett.* **2012**, *317–318*, 44–55. [[CrossRef](#)]
65. Parente, M.; Bishop, J.L.; Saranathan, A.M.; Szykiewicz, A.; Fenton, L. Detection of bassanite in the north polar dunes of Mars and implications for aqueous activity. In Proceedings of the 53rd Lunar and Planetary Science Conference (LPSC 2022), Houston, TX, USA, 7–11 March 2022; Volume 53, abst. no. 2342.
66. Szykiewicz, A.; Bishop, J.L.; Fenton, L.; Parente, M. Evidence for groundwater activity and sulfate origin in the basal unit and Olympia Undae dunes on Mars. In Proceedings of the 53rd Lunar and Planetary Science Conference (LPSC 2022), Houston, TX, USA, 7–11 March 2022; Volume 53, abst. no. 1615.
67. Cardenas, B.T.; Lamb, M.P. Paleogeographic reconstructions of an ocean margin on Mars based on deltaic sedimentology at Aeolis Dorsa. *J. Geophys. Res. Planets* **2022**, *127*, e2022JE007390. [[CrossRef](#)]
68. Feldman, W.C.; Pathare, A.; Maurice, S.; Prettyman, T.H.; Lawrence, D.J.; Milliken, R.E.; Travis, B.J. Mars Odyssey neutron data: 2. Search for buried excess water ice deposits at nonpolar latitudes on Mars. *J. Geophys. Res. Planets* **2011**, *116*, E11009. [[CrossRef](#)]
69. Feldman, W.C.; Bourke, M.C.; Elphic, R.C.; Maurice, S.; Prettyman, T.H.; Lawrence, D.J.; Hagerty, J.J. Constraints on the structure and composition of sand dunes within Olympia Undae using Mars Odyssey neutron spectrometer data. In Proceedings of the 38th Lunar and Planetary Science Conference (LPSC 2007), Houston, TX, USA, 12–16 March 2007; Volume 38, abst. no. 2311.
70. Martín-Torres, F.J.; Zorzano, M.-P.; Valentín-Serrano, P.; Harri, A.-M.; Genzer, M.; Kemppinen, O.; Rivera-Valentin, E.-G.; Jun, I.; Wray, J.; Madsen, M.B.; et al. Transient liquid water and water activity at Gale crater on Mars. *Nat. Geosci.* **2015**, *8*, 357–361. [[CrossRef](#)]
71. Bish, D.L.; Carey, J.W.; Vaniman, D.T.; Chipera, S.J. Stability of hydrous minerals on the Martian surface. *Icarus* **2003**, *164*, 96–103. [[CrossRef](#)]
72. Siebach, K.L.; Grotzinger, J.P. Volumetric estimates of ancient water on Mount Sharp based on boxwork deposits, Gale crater, Mars. *J. Geophys. Res. Planets* **2014**, *119*, 189–198. [[CrossRef](#)]

73. Sutter, B.; McAdam, A.C.; Mahaffy, P.R.; Ming, D.W.; Edgett, K.S.; Rampe, E.B.; Eigenbrode, J.L.; Franz, H.B.; Freissinet, C.; Grotzinger, J.P.; et al. Evolved gas analyses of sedimentary rocks and eolian sediment in Gale crater, Mars: Results of the Curiosity rover's sample analysis at Mars instrument from Yellowknife Bay to the Namib Dune. *J. Geophys. Res. Planets* **2017**, *122*, 2574–2609. [[CrossRef](#)]
74. Czarnecki, S.; Hardgrove, C.; Gasda, P.J.; Gabriel, T.S.J.; Starr, M.; Rice, M.S.; Frydenvang, J.; Wiens, R.C.; Rapin, W.; Nikiforov, S. Identification and description of a silicic volcanoclastic layer in Gale crater, Mars, using active neutron interrogation. *J. Geophys. Res. Planets* **2020**, *125*, e2019JE006180. [[CrossRef](#)]
75. King, P.L.; McLennan, S.M. Sulfur on Mars. *Elements* **2010**, *6*, 107–112. [[CrossRef](#)]
76. Ehlmann, B.L.; Edwards, C.S. Mineralogy of the Martian surface. *Ann. Rev. Earth Planet. Sci.* **2014**, *42*, 291–315. [[CrossRef](#)]
77. Franz, H.B.; McAdam, A.C.; Ming, D.W.; Freissinet, C.; Mahaffy, P.R.; Eldridge, D.L.; Fischer, W.W.; Grotzinger, J.P.; House, C.H.; Hurowitz, J.A.; et al. Large sulfur isotope fractionations in Martian sediments at Gale crater. *Nat. Geosci.* **2017**, *10*, 658–663. [[CrossRef](#)]
78. Bristow, T.F.; Grotzinger, J.P.; Rampe, E.B.; Cuadros, J.; Chipera, S.J.; Downs, G.W.; Fedo, C.M.; Frydenvang, J.; McAdam, A.C.; Morris, R.V.; et al. Brine-driven destruction of clay minerals in Gale crater, Mars. *Science* **2021**, *373*, 198–204. [[CrossRef](#)] [[PubMed](#)]
79. Seeger, C.H.; Grotzinger, J.P. Diagenesis of the clay-sulfate stratigraphic transition, Mount Sharp group, Gale crater, Mars. *J. Geophys. Res. Planets. in press*.
80. Martin, P.E.; Farley, K.A.; Malespin, C.A.; Mahaffy, P.R.; Edgett, K.S.; Gupta, S.; Dietrich, W.E.; Malin, M.C.; Stack, K.M.; Vasconcelos, P.M. Billion-year exposure ages in Gale crater (Mars) indicate Mount Sharp formed before the Amazonian period. *Earth Planet. Sci. Lett.* **2021**, *554*, 116667. [[CrossRef](#)]
81. Schwenzer, S.P.; Abramov, O.; Allen, C.C.; Bridges, J.C.; Clifford, S.M.; Filiberto, J.; Kring, D.A.; Lasue, J.; McGovern, P.J.; Newsom, H.E.; et al. Gale crater: Formation and post-impact hydrous environments. *Planet. Space Sci.* **2012**, *70*, 84–95. [[CrossRef](#)]
82. Knoll, A.H.; Grotzinger, J. Water on Mars and the prospect of Martian life. *Elements* **2015**, *2*, 169–173. [[CrossRef](#)]
83. Benison, K.C.; Karmanocky, F.J., III. Could microorganisms be preserved in Mars gypsum? Insights from terrestrial examples. *Geology* **2014**, *42*, 615–618. [[CrossRef](#)]
84. Parnell, J.; Lee, P.; Cockell, C.S.; Osinski, G.R. Microbial colonization in impact-generated hydrothermal sulphate deposits, Haughton impact structure, and implications for sulphates on Mars. *Int. J. Astrobiol.* **2004**, *3*, 247–256. [[CrossRef](#)]

**Disclaimer/Publisher's Note:** The statements, opinions and data contained in all publications are solely those of the individual author(s) and contributor(s) and not of MDPI and/or the editor(s). MDPI and/or the editor(s) disclaim responsibility for any injury to people or property resulting from any ideas, methods, instructions or products referred to in the content.